EINDHOVEN UNIVERSITY OF TECHNOLOGY

Eindhoven University of Technology

MASTER

Dream beam

from pancake to waterbag

van Oudheusden, T.

Award date:
2006

Link to publication

Dream Beam

from pancake to waterbag

T. van Oudheusden

Afstudeerbegeleider:
dr. ir. O.J. Luiten

Afstudeercommissie:
dr. ing. F.B. Kiewiet
prof. dr. K.A.H. van Leeuwen
dr. ir. O.J. Luiten (voorzitter)
dr. ir. P.P.A.M. van der Schoot
prof. dr. M.J. van der Wiel

TU/e technische universiteit eindhoven

faculteit Technische Natuurkunde

capaciteitsgroep Fysica en Toepassingen van Versnellers

Abstract

There are many applications of accelerated ultra-short, high-brightness electron bunches. One application highlighted in this report is time-resolved electron diffraction. For this application electron bunches with a charge of $1\,pC$, a radius less than $100\,\mu m$, and a duration less than $100\,fs$ would be ideal to study many ultra-fast physical, biological, and chemical processes on the timescale of atomic motions. Such bunches have not been realized in practice yet. In this report a way to create such short bunches is presented.

In the quest for ultra-short, high-brightness electron bunches it was already realized a long time ago that uniformly charged ellipsoidal bunches would be ideal. These bunches are called "waterbags". Because of their linear space charge fields waterbag bunches can in principle be focussed transversely and longitudinally to any desired dimension with electro-magnetic lenses, that have sufficiently linear fields. Because of these ideal focussing properties a charged particle beam consisting of waterbag bunches is also referred to as "Dream Beam".

In 2004 a scheme has been proposed to create these waterbags in practice [1]. Under certain conditions an initially flat bunch, a so-called pancake bunch, will evolve into a waterbag bunch driven by its own space charge fields. Nowadays ultra-short laser pulses of several tens of femteseconds duration are available, which can be used to create pancake bunches by photoemission. In order to have these pancake bunches evolve into waterbags certain conditions have to be fulfilled, regarding the magnitude and the shape of the surface charge density of the pancake bunch, and the strength of the acceleration field.

The surface charge density distribution needs to be hemisphere-like. In this report two commercially available devices are proposed for shaping of the transverse laser intensity profile. Preliminary results are presented of profile shaping of a continuous HeNe laser beam using neutral density filters, and of spatial filtering of ultra-short Ti:S laser pulses.

The other two conditions lead to constraints on the parameter space of the magnitude of the surface charge density and the acceleration field strength. In this report this parameter space is explored by particle tracking simulations to find realistic limits for the acceleration field strength as a function of the magnitude of the surface charge density. The results of the simulations confirm the analytical limits. However, more research is necessary on the quantification of the resemblance of a bunch to a waterbag.

To demonstrate the creation of waterbag bunches in practice a $100\,kV$ DC photogun has been designed. During training of this photogun a maximum voltage of $73\,kV$ has been reached, corresponding to an acceleration field of $8.6\,MV/m$ at the cathode surface. Both back- and front-illumination have been done with this photogun. By back-illumination of a $30\,nm$ thick silver film with ultra-short ($35\,fs$) laser pulses of $800\,nm$, bunches are measured with charges up to $(0.6 \pm 0.2)\,pC$. However, due to a 1 nm chromium layer between the fused silica substrate and the silver film, the photocathode is damaged during photoemission experiments. Also photoemission by front-illumination has been done. Ultra-short ($50\,fs$) $266\,nm$ UV laser

pulses have been used to photoemit electrons from bulk copper. The intensity of the laser pulses has turned out to be so high that photoemission has taken place in the space charge limited regime: the charge of a bunch is an increasing function of the acceleration field. Bunch charges up to 14 pC are measured when applying an acceleration field of 6.3 MV/m.

Many steps in preparation of the experimental realization of waterbag bunches have been taken: a theoretical basis is given, particle tracking simulations have been done, and a 100 kV DC photogun has been designed, constructed, and tested. The last preparation step is shaping of the transverse laser intensity profile. Then all ingredients are present to create waterbag bunches in practice.

Contents

Chapter 1

Introduction

1.1 Applications of high-brightness electron bunches

Applications of ultra-short, high-brightness electron bunches are extensive: from the generation of intense Terahertz radiation to time-resolved imaging of physical, chemical and biological processes.

Generation of Coherent Transition Radiation (CTR) can be accomplished by an electron bunch which passes a discontinuity in permittivity. The spectrum of this radiation is extremely flat and reaches from far below to far beyond the THz-regime. This provides a new concept of an intense compact THz source [2]. If the length of the electron bunch is shorter than the wavelength of the transition radiation, then the emitted radiation of each individual electron will add up coherently. It is predicted by theory that 100 pC bunches shorter than 100 fs, and an energy of 5 MeV will generate THz radiation of more than 5.7 MV/cm.

With ultra-short electron bunches time resolved imaging of ultra-fast processes can be accomplished by electron diffraction. This technique provides time-resolved study of physical, chemical, and biological processes on the timescale of atomic motion. Examples are phase-transitions [3], transitions of molecular structures [4], and the action of proteins [5]. For single-shot, time-resolved electron diffraction electron bunches are required of typically 1 pC charge, 100 μm radius, 100 fs duration, and 100 keV energy.

Another application of ultra-short, high-brightness electron bunches is the X-ray Free Electron Laser (XFEL). Electron bunches can also be used in "pump & probe" experiments, such as the excitation of charge carriers in polymers.

These examples are just the tip of an iceberg. Ultra-short electron bunches will provide scientists of many fields a new tool for developing their knowledge about our world. The quest for ultrashort, high-brightness electron bunches is worth the effort.

1.2 The problem of the creation of high-brightness electron bunches

When creating high-brightness electron bunches one major problem has to be overcome: space charge forces. The electrons in the bunch repel each other as a result of Coulomb's force. Because for applications generally short bunches with a small spotsize, lots of charge, and a small energy spread are required, the bunch has to be focussed transversely and longitudinally. However, due to space charge forces the bunch grows and deforms generally in an irreversible

way, so that it can not be compressed to its original dimensions. In order to create an as short as possible bunch the "traditional" solution (see section 1.3) is to accelerate the bunch as quickly as possible to relativistic velocities, because at these velocities the bunch explosion is slowed down. A "novel" approach (see section 1.4) is to create a charge distribution which can always be focussed after being accelerated. This solves the problem of space charge density distribution.

1.3 Traditional approach: quick acceleration

In the traditional approach the problem is said to be space charge density. The solution is to slow down the bunch explosion as much as possible by accelerating the bunch to relativistic velocities as quickly as possible. However, in this way one is fighting the symptom (bunch explosion) rather than solving the problem.

To make clear how this concept works, consider the acceleration of an electron. The relativistic version of Newton's second law reads as follows:

$$\vec{F} = \frac{d}{dt}\left(\gamma m \vec{v}\right),\tag{1.1}$$

where $\vec{F}$ is a force acting on a particle with rest mass m and velocity $\vec{v}$, and $\gamma = \left(1 - \left(\frac{v}{c}\right)^2\right)^{-1/2}$ the Lorentz factor with c the velocity of light, and $v = |\vec{v}|$.

For the two cases $\vec{F}$ parallel to $\vec{v}$ and $\vec{F}$ perpendicular to $\vec{v}$ the following expressions for the acceleration are obtained from equation (1.1):

$$a_{\parallel} = \frac{F_{\parallel}}{\gamma^3 m},\tag{1.2}$$

$$a_{\perp} = \frac{F_{\perp}}{\gamma m}.\tag{1.3}$$

In the longitudinal direction only Coulomb forces are acting. It is clear that the force is reduced by a factor γ^3 in the longitudinal direction resulting in a smaller acceleration and thus a slower bunch explosion.

In the transverse direction also magnetic forces show up. Consider the total force on an electron in a cylindrical beam with varying radial density $n(r)$. For the electric field $\vec{E}$ inside the beam the following equation holds:

$$\vec{E} = \vec{e}_r \frac{q}{\varepsilon_0 r} \int_0^r r' n(r') dr',\tag{1.4}$$

where q is the charge of the particle considered, and ε_0 is the permittivity of vacuum. For the magnetic field $\vec{B}$ inside the beam the following equation holds:

$$\vec{B} = \vec{e}_{\phi} \frac{q v \mu_0}{r} \int_0^r r' n(r') dr',\tag{1.5}$$

where v is the velocity of the particle considered, and μ_0 is the permeability of vacuum. These two fields lead to a radial Lorentz force F_r which is given by:

$$F_r = q\left(E_r - vB_\phi\right) = qE_r\left(1 - \frac{v^2}{c^2}\right) = \frac{qE_r}{\gamma^2}, \tag{1.6}$$

where $\varepsilon_0\mu_0 = 1/c^2$ is used. So besides the factor γ in equation (1.3) the total radial force on an electron in a beam is reduced by an additional factor γ^2 due to the magnetic force, which opposes the Coulomb repulsion. In the transverse direction the force is thus also reduced by a factor γ^3 as is the case in the longitudinal direction. As a result the bunch explosion is slowed down in all directions when the bunch travels at relativistic velocities. In the limit $v \to c$ the acceleration due to space charge forces goes to zero and the bunch retains its dimensions.

1.4 Novel approach: the waterbag bunch

In the traditional approach much effort is needed to create higher and higher acceleration gradients to keep bunch dimensions more or less under control. The real problem however is not being solved. Only the symptom (bunch growth) is controlled. In the novel approach first the problem is defined properly: not the magnitude of space charge density itself is the real problem, but its <u>distribution</u>. This problem is solved by creating a bunch whose space charge density distribution gives rise to fully controllable, i.e. linear, space charge fields. This is the case for a 3-D ellipsoid with a uniform charge density, also called a **waterbag** bunch. Of course the waterbag bunch still explodes due to Coulomb's force, but it retains an ellipsoid and thus its linear space charge fields. For a homogeneous sphere, which is a special kind of ellipsoid, this can be imagined easily. Figure 1.1 shows a cross-section of a sphere with initial radius R. Electrons with a total charge Q are distributed homogeneously inside the sphere and are initially at rest. The electric field for $r \leq R$ is well-known: $E_r(r) = \frac{Q}{4\pi\varepsilon_0 R^2}\frac{r}{R}$. The electric field is thus a linear function of r and is pointing in the radial direction. As a result the velocity field of the charged particles is also a linear function of r. The sphere is thus expanding radially and the charge distribution remains homogeneous, as visualized in the right panel of figure 1.1.

Because of its linear space charge fields a waterbag bunch can be compressed transversely and longitudinally to any desired dimension with electro-magnetic lenses, that have sufficiently linear fields. Realization of a waterbag bunch is truly a "Dream Beam" come true. This report is about the creation of such a Dream Beam.

A waterbag bunch can be created by blow out of an ultra-thin sheet of electrons, referred to as pancake [6]. Under certain conditions, concerning the strength of the acceleration field and the magnitude and distribution of the initial surface charge density, a pancake should evolve into a waterbag [1].

1.5 Scope

This report is about the creation of a Dream Beam, a novel concept of creating high-brightness electron bunches. The problem of space charge is properly defined and the "traditional" and "novel" approaches are shortly described earlier in this chapter. In the next chapter it is explained how electron bunches can be described in phase space. Also the terms "emittance" and "brightness" are explained. Chapter 3 is about the theory of the creation of waterbag bunches, also referred to as Dream Beam. First it is defined what a waterbag bunch is and

t = 0   t > 0
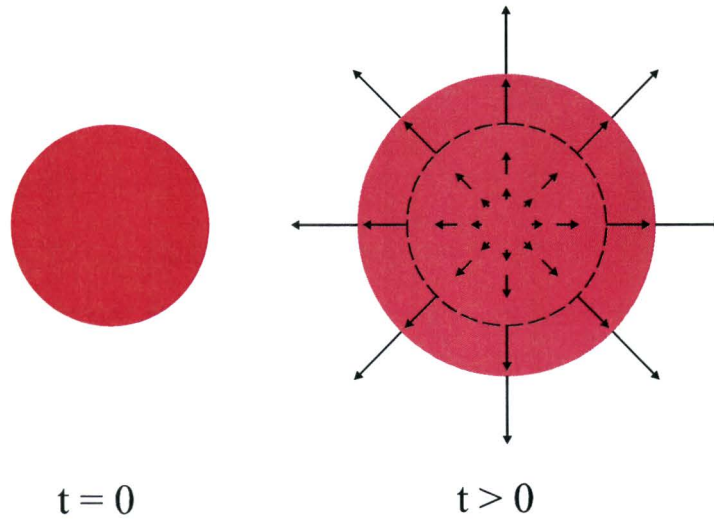
Figure 1.1: *cross-section of a homogeneously charged sphere. At t = 0 the charged particles are at rest. The linear electric field inside the sphere leads to a velocity field of the charged particles which is a linear function of r and is pointing in the radial direction. This velocity field is indicated by the arrows in the right panel. As a result the sphere is expanding radially while retaining a homogeneous charge density distribution. The dashed contour indicates the shape of the bunch as it was at t = 0.*

its characteristics are described. Then a practical scheme to realize these waterbags is presented. Necessary conditions on the acceleration field strength, and on the initial magnitude and initial distribution of the surface charge density, are presented and explained. Then in chapters 4 and 5 an attempt is made to convince the reader that this Dream Beam could be realized in practice, which would make a dream coming true. First in chapter 4 the parameter space of the acceleration field strength versus the magnitude of the surface charge density is explored by particle tracking simulations. Then in chapter 5 first steps of necessary laser profile shaping (to obtain the required initial charge density distribution) are presented.

In chapter 6 the design of a 100 kV DC photogun is presented, which will be used to demonstrate the waterbag concept.

A way of longitudinal compression or time-focussing of waterbag bunches with a pillbox RF cavity is described in chapter 7. Results of simulations with a 1 pC bunch are presented.

With the 100 kV DC photogun measurements of quantum efficiencies of linear photoemission by front-illumination and third order photoemission by back-illumination have been done. Results of first measurements are presented in chapter 8.

Finally in chapter 9 conclusions and an outlook for the progress of the project are presented.

Chapter 2

Phase space

A many-particle system, such as an electron bunch, is fundamentally described in phase space. Closely connected to the phase space are the quantities "emittance" (the focusability of the bunch) and "brightness"(beam current density per unit solid angle and per unit energy spread). These quantities are for many applications the most important parameters and provide a way to compare beam qualities. Moreover, the brightness is an absolute measure of the quality of a bunch.

In this chapter it is first explained how an electron bunch can be described in phase space. In section 2.2 definitions of emittance are presented, and a practical meaning of emittance is described. Next, in section 2.3 definitions of brightness are given. Finally, in section 2.4 the "thermal emittance" is treated, which is the minimum possible emittance of an electron bunch determined by the photoemission process.

2.1 Phase space

If the forces acting on the electrons in a bunch can be derived from a potential which is independent of the momenta of the electrons, then the bunch as a whole is a Hamiltonian system. This is the case if [7]:

- wave mechanical effects can be ignored;

- electromagnetic radiation can be neglected;

- there are no close-range interactions between the electrons (collisions);

- there are no long-range interactions between the electrons which depend on their velocity.

Because of its definition a Hamiltonian system is uniquely described by its Hamiltonian, which is a function of the conjugate pairs of coordinates r_i and p_i, where $i = x, y, z$. The position is denoted by $\vec{r}$, and the momentum by $\vec{p} = \gamma m \vec{v}$, with the Lorentz factor $\gamma = \frac{1}{\sqrt{1-v^2/c^2}}$, rest mass m, and velocity $\vec{v}$. The motion of each electron in a bunch can be represented by its trajectory in the 6-D phase space $(\vec{r}, \vec{p})$. If this is done for all electrons in the bunch, then at every point in time t the bunch is characterized by a set of points in the 6-D phase space. The bunch can then be described by a density distribution function $f(\vec{r}, \vec{p}, t)$ in the 6-D

phase space. From the continuity equation it follows that the local density f in phase space is a conserved quantity. This is known as Liouville's theorem. The hypervolume enclosing a chosen group of points is constant in time: its shape may vary, but the volume enclosed remains constant.

The notion of a beam already indicates that there is a preferred direction of motion: the longitudinal velocity is much larger then the transverse velocities. The Hamiltonian can then be split up in two terms: one representing the longitudinal motion, and the other representing the transverse motion. If for all separate particles the motion associated with each degree of freedom is independent of the other two, then the Hamiltonian can be split up into a sum of three terms. Each term is representing one degree of freedom, that is one pair (r_i, p_i) where $i = x, y, z$. The density distribution function then equals the product of the three projected density distributions: $f(x, p_x, y, p_y, z, p_z) = f_x(x, p_x) f_y(y, p_y) f_z(z, p_z)$. The motions of the electrons can then be represented in three separate phase spaces (one for each degree of freedom x, y, z). As a result the area of the projection of the full 6-D distribution on each of these phase spaces is a conserved quantity. It should be noted however that this decoupling is in practice generally not complete, but for weak coupling it is generally assumed that a beam can be accurately described in three separate 2-D phases.

2.2   Emittance

2.2.1   Definitions

The hyperemittance equals the hypervolume V_{6D}, occupied by the bunch in the 6-D phase space, divided by π^3. This is however an artificial definition and is in practice never used. As explained in the previous section the full 6-D phase space of an accelerated bunch can be separated in a (4-D) transverse and a (2-D) longitudinal phase space. As a consequence the hyperemittance can be split up in the same way. If, furthermore, the transverse phase space is separable in two pairs of conjugate coordinates, then also the transverse emittance can be split up. Thus three emittances are obtained: ε_x, ε_y, and ε_z. The emittance equals the area A_p of the projection of the phase space density distribution on the corresponding 2-D phase space, divided by πmc:

$$\varepsilon_i \equiv \frac{A_{p,i}}{\pi mc}, \text{ with } i = x, y, z. \tag{2.1}$$

For hard-edged bunches the area is generally taken to be that of the smallest ellipse which is enclosing all particles. In reality however bunches generally do not have sharp edges. The lengths of the semi-axes of the ellipse in, for instance, the (x, p_x) phase space are then estimated by σ_x and σ_{p_x} respectively, where $\sigma_a^2 \equiv <(a - <a>)^2>$ is the variance of quantity a. In this way the RMS-emittance is obtained, which is defined as follows:

$$\varepsilon_x = \frac{1}{mc}\sigma_x\sigma_{p_x}, \tag{2.2}$$

It is assumed that the primary axes of the ellipse in the phase space are coincident with the x- and p_x-axis. Generally this is not the case and a cross-term has to be taken into account. The general definition of the normalized RMS-emittance $\varepsilon_{n,x}$, which is a Lorentz invariant quantity, is given by:

$$\varepsilon_{n,x} = \frac{1}{mc}\sqrt{< (x- < x >)^2 >< (p_x- < p_x >)^2 > - < (x- < x >)(p_x- < p_x >) >^2}. \quad (2.3)$$

where the brackets $< >$ indicate an average over the entire bunch.

In practice the emittance is not measured in the phase space, but in the so-called configuration or trace space. That is, not the transverse momenta are measured, but the paraxial angles $x' = \frac{dx}{dz}$ and $y' = \frac{dy}{dz}$. A paraxial approximation can be applied if the longitudinal velocity is much greater than the transverse velocities: $v_x, v_y \ll v_z \approx c$. Then $\beta_x \approx \beta\frac{v_x}{v_z} \approx \beta x'$ and $\beta_y \approx \beta y'$, with $\beta = \frac{v}{c} \approx \beta_z$. In the configuration space (x, x') the emittance is given by:

$$\varepsilon_{n,x} = \sqrt{< (x- < x >)^2 >< (\gamma\beta x'- < \gamma\beta x' >)^2 > - < (x- < x >)(\gamma\beta x'- < \gamma\beta x' >) >^2}. \quad (2.4)$$

For non-skewed distributions the RMS-emittances are thus given by:

$$
\begin{aligned}
\varepsilon_{n,x} &= \gamma\beta\sigma_x\sigma_{x'}; \\
\varepsilon_{n,y} &= \gamma\beta\sigma_y\sigma_{y'}; \\
\varepsilon_{n,z} &= \sigma_z\sigma_{\gamma\beta} = \frac{1}{mc}\sigma_t\sigma_u,
\end{aligned}
\quad (2.5)
$$

where U is the total energy of an electron in the bunch. For a beam the energy of an electron is much larger than the energy spread, so that $\sigma_{\gamma\beta} = \frac{\partial(\gamma\beta)}{\partial\gamma}\sigma_\gamma = \frac{\sigma_\gamma}{\beta}$. The transverse normalized RMS-emittance $\varepsilon_{n,x}$ or $\varepsilon_{n,y}$ equals $\gamma\beta$ times the RMS bunch radius times the RMS angular spread. If the factor $\gamma\beta$ is left out, the so-called geometrical emittance is obtained. This emittance is a decreasing function of the energy, an effect which is called "adiabatic damping". The longitudinal normalized RMS-emittance $\varepsilon_{n,z}$ equals $\frac{1}{mc}$ times the RMS bunch duration times the RMS energy spread. A high-quality bunch of N electrons is short and has a small radius, a small divergence, and a small energy spread. A high-quality bunch is thus characterized by small emittances.

2.2.2 Practical meaning

The emittance is a measure for the focusability of an electron beam. When realizing that the angular spread $\sigma_{x'}$ is maximally equal to unity, then it is easy to see that a beam of given emittance $\varepsilon_{n,x}$ can be focussed to a minimum spot size $\sigma_x \geq \frac{\varepsilon_{n,x}}{\gamma\beta}$, i.e. the value of the geometrical emittance. If smaller spot sizes have to be realized the emittance of the beam has to be decreased.

A nice way to visualize this, is by considering focusing of a laminar beam and of a non-laminar beam, as illustrated in figure 2.1. A perfectly laminar beam can be focused with an ideal lens to a point of zero dimension[1]. A perfectly parallel laminar beam of finite spot size σ_x has no spread of transverse velocity: $\sigma_{p_x} = 0$. In the focal point there is a finite transverse velocity spread, but the spot size equals zero. In both cases the emittance is thus zero. In the transverse phase space such a beam is characterized by an infinitely straight line through the origin. The area of this line and thus the emittance equals zero.

---

[1]Fundamental limits, like the diffraction limit, are disregarded as the intention of this section is only to illustrate how size and velocity spread determine the emittance of a beam.
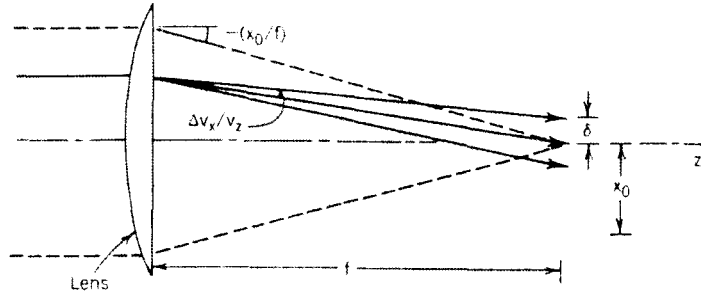
Figure 2.1: *non-laminar beam with at all positions in the cross-section of the beam a transverse velocity spread Δv_x. The beam is focused with an ideal lens to a minimum spot size δ, whereas a laminar beam is focused to a point of zero dimension. Figure from reference [8].*

Consider next a non-laminar beam which has at all positions in its cross-section a transverse velocity spread Δv_x, and which is focused to a spot of non-zero radius δ, as indicated in figure 2.1. The velocity spread in the non-laminar beam is reflected by a non-zero area in the transverse phase space and thus a non-zero emittance. The shorter the focal length f of the lens, the smaller δ will be. There is however a minimum value of δ, determined by the emittance.

2.3   Brightness

The usual definition of brightness (also referred to as spectral brightness or brilliance) is current density per unit solid angle and per unit energy spread, which can also be written in terms of emittances:

$$B_n = \frac{1}{\gamma^2 \beta^2} \frac{I}{A^{RMS} \, \Omega^{RMS} \, \sigma_U} = \frac{Q}{mc \, \varepsilon_{n,x} \, \varepsilon_{n,y} \, \varepsilon_{n,z}}, \tag{2.6}$$

where $I = \frac{Q\beta c}{\sigma_z}$ is the current of the bunch, A^{RMS} is the RMS-area of the projection of the bunch on the (x,y)-plane, Ω^{RMS} is the RMS solid angle, and Q is the of charge the bunch. Note that the brightness thus defined is a Lorentz invariant quantity. The general definition of brightness given above is however seldom used. Usually the brightness is split up in a normalized transverse brightness $B_{n,\perp}$ and a longitudinal brightness $B_{n,\parallel}$:

$$B_{n,\perp} = \frac{1}{\gamma^2 \beta^2} \frac{I}{A^{RMS} \, \Omega^{RMS}} = \frac{I}{\varepsilon_{n,x} \, \varepsilon_{n,y}}; \tag{2.7}$$

$$B_{n,\parallel} \propto \frac{I}{\sigma_U}, \tag{2.8}$$

However also another definition of brightness is often used, which is $(2\pi)^3$ times smaller than the brightness as defined by equation (2.6):

$$B_n^G = \frac{Q}{(2\pi)^3 mc \, \varepsilon_{n,x} \, \varepsilon_{n,y} \, \varepsilon_{n,z}}; \tag{2.9}$$

$$B_{n,\perp}^G = \frac{I}{(2\pi)^2 \varepsilon_{n,x} \, \varepsilon_{n,y}}. \tag{2.10}$$

These are in fact peak brightnesses as is explained in the following. The factor $\frac{1}{(2\pi)^3}$ is a result of the assumption that the distribution in 6-D phase space is Gaussian in all 6 dimensions:

$$f\left(x, p_x, y, p_y, z, p_z\right) = f_0 \exp\left[-\left(\frac{x^2}{2\sigma_x^2} + \frac{p_x^2}{2\sigma_{p_x}^2} + \frac{y^2}{2\sigma_y^2} + \frac{p_y^2}{2\sigma_{p_y}^2} + \frac{z^2}{2\sigma_z^2} + \frac{p_z^2}{2\sigma_{p_z}^2}\right)\right], \tag{2.11}$$

with $f_0 = f\left(\vec{0}, \vec{0}\right)$. Integration of the phase space density distribution gives the number of particles N in the bunch, leading to:

$$f_0 = \frac{N}{(2\pi)^3 \sigma_x \sigma_{p_x} \sigma_y \sigma_{p_y} \sigma_z \sigma_{p_z}}. \tag{2.12}$$

The normalized peak brightness is then given by $B_n^G = e f_0 m^2 c^2$.

2.4 Thermal emittance

Photoemitted electrons start off with non-zero energy spread and angular spread, which determines the starting emittance of the bunch. It is the minimum possible emittance and is called the "thermal emittance" ε_{th}. The thermal emittance can be estimated by assuming a thermalized distribution of electrons without any correlation between position and momentum. A measure for the standard deviation of the momentum is then $\sigma_{p_i} = \sqrt{mk_BT}$ with $i = x, y, z$, where m is the rest mass of an electron, k_B is Boltzmann's constant, and T is the effective temperature of the electrons that are emitted from the cathode. The minimal thermal emittance is due to the finite excess energy of the photoemitted electrons, combined with a finite initial angular distribution.

The mean energy of the electrons equals the difference between the energy of the incident photons $\hbar\omega$ and the effective work function Φ_e of the photocathode. The minimal emittance that can be achieved when creating bunches by photoemission is then given by:

$$\varepsilon_{n,x}^{th} = \frac{1}{mc} \sigma_x \sigma_{p_x} = \sigma_x \sqrt{\frac{\hbar\omega - \Phi_e}{mc^2}}. \tag{2.13}$$

The effective work function of a metal photocathode is generally lower than the real work function due to the presence of an electric field. This is called the Schottky effect which is described by:

$$\Phi_e = \Phi - \sqrt{\frac{e^3 E_{acc}}{4\pi\varepsilon_0}}, \tag{2.14}$$

where Φ is the work function of the metal, E_{acc} is the local acceleration field, and ε_0 is the permittivity of vacuum. For linear photoemission ($U_{\hbar\omega}$ =4.65 eV) from flat, clean copper

surfaces (Φ =4.6 eV) at room temperature the thermal emittance is typically several tenths of mm mrad for a hard-edged laser spot of 1 mm radius. For an electric field strength of 100 kV/cm at the cathode the thermal emittance $\varepsilon_{n,x}^{th} = 0.58$ mm mrad.

Chapter 3

From pancake to waterbag

As explained in the introduction a uniformly charged ellipsoidal bunch, called a "waterbag" bunch, is desirable because of its linear space charge fields. This kind of bunch can be compressed longitudinally and transversely to any desired dimension with charged particle optics that have sufficiently linear electro-magnetic fields. In this chapter it is explained how such an ideal electron bunch can be created. The idea is that an initially flat bunch, also called "pancake" bunch, evolves into a waterbag bunch driven by its own space charge fields. First in section 3.1 waterbag characteristics are described. Its space charge field is given and its phase space characteristics are presented. In section 3.2 it is shown that an oblate spheroid (which has a length that is shorter than its diameter) evolves into a prolate spheroid (which has a length that is longer than its diameter). Finally in section 3.3 the waterbag recipe is presented. That is, it is explained how an ultra-flat spheroid can be approximated by a pancake bunch. Conditions on this pancake bunch and on the acceleration field are treated, which have to be fulfilled for the evolution of a pancake into a waterbag bunch. These conditions are leading to a parameter space of the magnitude of the surface charge density and the acceleration field strength.

3.1 Waterbag characteristics

A waterbag bunch is a hard-edged 3-D ellipsoid of uniform charge density. Its confining surface is given by:

$$\left(\frac{x}{A}\right)^2 + \left(\frac{y}{B}\right)^2 + \left(\frac{z}{C}\right)^2 = 1, \tag{3.1}$$

where A, B, and C, are the lengths of the semi-axes of the ellipsoid. Consider an ellipsoidal bunch of uniform charge density ρ_0 at rest (i.e. all electrons in the bunch have zero velocity) in its rest frame. The particle distribution n is given by:

$$n\left(\vec{r}\right) = H\left[1 - \left(\frac{x}{A}\right)^2 - \left(\frac{y}{B}\right)^2 - \left(\frac{z}{C}\right)^2\right], \tag{3.2}$$

where $H(x)$ is the Heaviside step function of x:

$$H\left(x\right) = \begin{cases} 0 & \text{, if } x < 0 \\ 1 & \text{, if } x \geq 0. \end{cases} \tag{3.3}$$
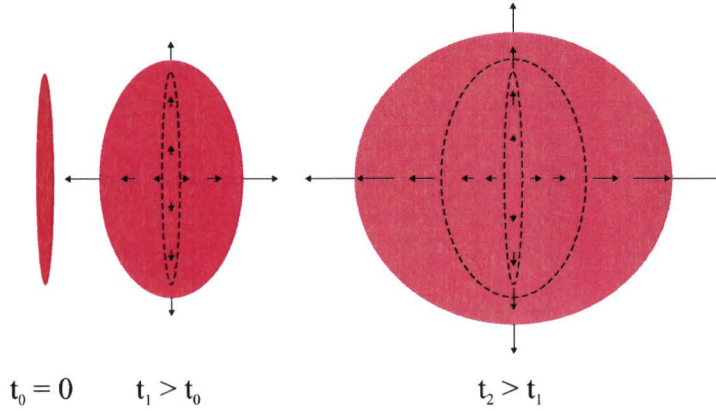
11

Figure 3.1: *cross-section of a homogeneously charged ellipsoid. The arrows indicate particle velocities. At $t_0 = 0$ the charged particles are at rest. The linear space charge field is leading to a linear velocity field of the charged particles. As a result the ellipsoid is expanding faster in the longitudinal than in the transverse direction as indicated for $t_1 > t_0$. However, the bunch keeps its homogeneous charge density distribution and thus its linear space charge field. At some time $t_2 > t_1$ the initial flat ellipsoid has expanded to a longitudinally stretched ellipsoid. The dashed contours indicate the shapes of the bunch as they were at previous times t_0 and t_1.*

The space charge field, that is the electric field inside the bunch, is given by [9]:

$$\vec{E}(x, y, z) = \frac{\rho_0}{\varepsilon_0} (M_x x, M_y y, M_z z), \tag{3.4}$$

where M_x, M_y, and M_z are geometrical constants, which are only depending on the dimensions of the ellipsoid A, B, and C. The space charge field is thus a linear function of position and is therefore leading to linear velocity-position correlations of the electrons in the bunch as depicted in figure 3.1. The 6-D phase space density distribution function $f(\vec{r}, \vec{p})$ normalized to the number of particles N in the bunch is generally given by:

$$f(\vec{r}, \vec{p}) = \frac{\rho_0}{e} n(\vec{r}) \delta(\vec{p} - \mathbf{D}\vec{r}), \tag{3.5}$$

where $\delta(x)$ the Dirac delta function of x. The 3×3 matrix $\mathbf{D}$ describes the coupling between spatial and momentum coordinates. For an expansion purely driven by linear space charge fields this matrix is thus diagonal. The 6-D phase space can then be split up in the three decoupled 2-D phase spaces (x, p_x), (y, p_y), and (z, p_z). A uniformly charged ellipsoid is thus characterized by straight lines through the origin in all the three 2-D phase spaces. Because of these linear velocity-position correlations an initially homogeneously charged ellipsoid remains homogeneous and thus retains a linear space charge field. In the introduction (section 1.4) this is explained for a homogeneous sphere, which is a special kind of ellipsoid. A uniform ellipsoid is the most general kind of bunch that has linear space charge fields. Because of these linear internal fields a uniformly charged ellipsoid can be compressed in all dimensions with linear charged particle optics.

3.2 Space charge fields in spheroids

In practice bunches are usually cylindrically symmetric. Cylindrically symmetric ellipsoids are called spheroids of which three kinds are distinguished:

- prolate, $A = B < C$;

- oblate, $A = B > C$;

- sphere, $A = B = C$.

The geometrical factors in equation (3.4) are given by [9]:

$$M_z = \frac{1 + \Gamma^2}{\Gamma^3} \left[\Gamma - \arctan\left(\Gamma\right) \right],$$
$$M_x = M_y = \frac{1}{2} \left(1 - M_z \right), \tag{3.6}$$

with $\Gamma \equiv \sqrt{A^2/C^2 - 1}$ the eccentricity of the ellipsoid. Note that the eccentricity defined in this way is real for an oblate spheroid and purely imaginary for a prolate spheroid. However M_z is real for both kinds of spheroids. For large eccentricities, i.e for $A = B \gg C$, $M_z \to 1$ and $M_x = M_y \to \frac{C}{A}\frac{\pi}{4}$ and the electric fields are given by:

$$
\begin{aligned}
E_x(x) &= \frac{3Q}{16\varepsilon_0 A^2}\frac{x}{A}; \\
E_y(y) &= \frac{3Q}{16\varepsilon_0 A^2}\frac{y}{A}; \\
E_z(z) &= \frac{3Q}{4\pi\varepsilon_0 A^2}\frac{z}{C},
\end{aligned}
\tag{3.7}
$$

where Q is the total charge of the bunch. Figure 3.2 shows a graph of the ratio $\frac{E_z(C)}{E_x(A)}$ as a function of $\frac{C}{A}$. The electric field components E_x and E_z are evaluated at the extremal points of the ellipsoid, i.e. at $x = A$ and $z = C$ respectively. From this figure it is clear that in an oblate spheroid the space charge field is stronger at $z = C$ than at $x = A$. Therefore a pancake-like oblate will evolve into a cigar-like prolate spheroid *due to its own space charge fields*. This is also indicated in figure 3.1. It is therefore concluded that waterbag bunches of any shape can be obtained by starting out with a very flat oblate spheroid. This suggest a way to realize waterbag bunches in practice, which is explained in the following section.

3.3 Waterbag recipe

In this section the subtitle of this report is explained: a waterbag bunch can be created by starting out with a pancake electron bunch.

When creating an electron bunch, e.g. by photoemission, it is practically impossible to realize a 3-D ellipsoid, because this requires 3-D shaping of the laser pulse. However, ultra-short laser pulse technology provides the possibility to create cylindrically symmetric bunches with a high aspect ratio, referred to as *pancakes*. Under certain conditions a pancake bunch will evolve
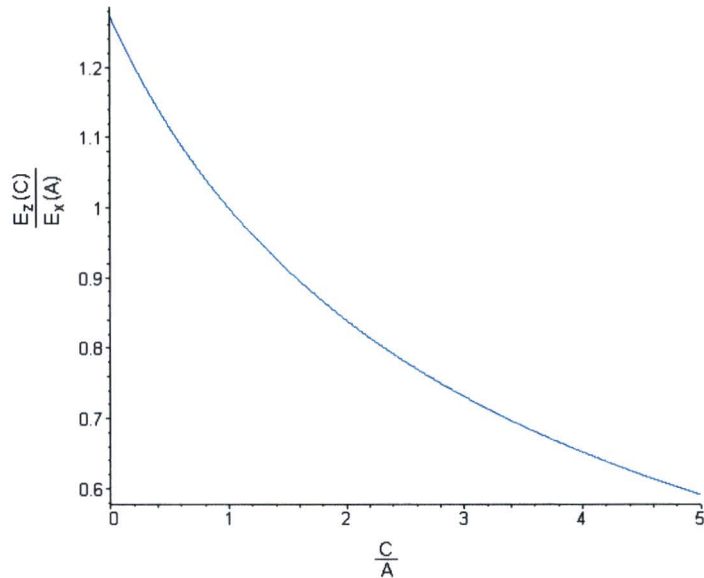
Figure 3.2: *ratio $\frac{E_z(C)}{E_x(A)}$ of the electric fields at the extremal points of a homogeneous spheroid as a function of $\frac{C}{A}$. The x-component of the electric field is evaluated at $x = A$ and the z-component at $z = C$.*

into a waterbag driven by its own space charge fields. This idea of "blow-out" of a short bunch to a waterbag was already mentioned by Serafini [10] in 1997. However, both the longitudinal and the transverse charge density distribution suggested in that reference are wrong. The correct distributions are given in reference [1]. It turns out that to realize the correct distribution in practice only 2-D (transverse) shaping of the ultra-short laser pulse is required, for which several technologies are available.

3.3.1 Pancake conditions

In theoretical astrophysics it was observed that a uniform prolate spheroid will collapse under its own weight into a flat disk, i.e. an oblate spheroid with $C = 0$ [11]. The driving force (gravitation) is linear like the (electrical) space charge force in a waterbag, but the direction is opposite. So this collapse is the time-reversed analog of the explosion of an electron bunch. The density distribution $\rho(r, z)$ of the flat disk (after the collapsing) is given by:

$$\rho(r, z) = \sigma_0 \sqrt{1 - (r/A)^2} \delta(z), \tag{3.8}$$

where σ_0 is the surface charge density at the center and $r = \sqrt{x^2 + y^2}$. Reversing this collapsing process implies that an ultra-thin sheet of electrons with a charge density distribution as given by equation (3.8) will evolve into a uniformly charged spheroid.

However, it is obvious that an infinitely thin flat disk (a 2-D body) will not evolve into any 3-D body. So it is not completely true that the evolution of an ultra-thin sheet of electrons can be seen as the reverse of the collapse process. Contrary to the flat disk the ultra-thin sheet has a small, but finite thickness. Furthermore, the sheet is created in time by photoemission from a metal surface. This has three consequences.
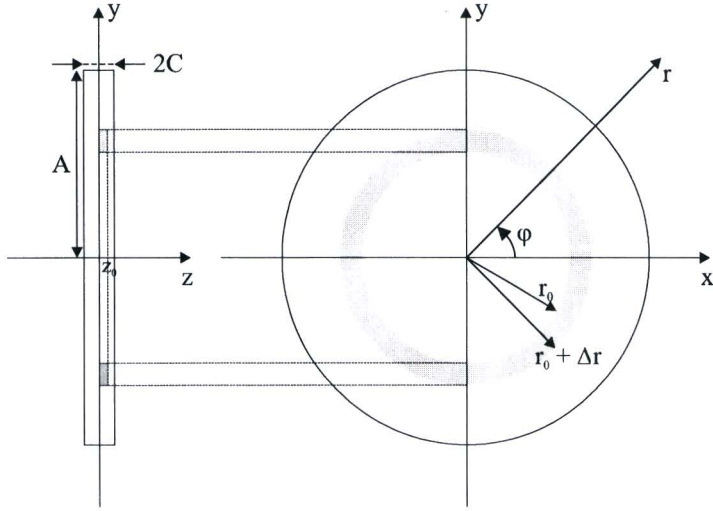
Figure 3.3: *side view and front view of a pancake bunch in a polar coordinate system. The pancake bunch has radius A and length 2C. The gray parts of the bunch indicate the volume to which Gauss's law is applied to calculate the electric field at a point (r_0, z_0) inside the bunch.*

1. The initial charge density distribution does not fulfill equation (3.8): the Dirac delta function $\delta(z)$ has to be replaced by a realistic longitudinal distribution function $\lambda(z)$.

2. The front side of the ultrathin sheet is created earlier than the back side.

3. Image-charge forces are counteracting the acceleration field during initiation of the bunch.

In the following these three points are examined in more detail.

Longitudinal charge density function

A pancake electron bunch is a bunch with a small aspect ratio [6]: $\frac{C}{A} \ll 1$, where C is the half-length of the bunch, and A is its radius. The rest frame bunch length is thus much smaller than the bunch radius. Figure 3.3 shows a schematic of a pancake bunch in a polar coordinate system.

The longitudinal component of the electric field inside a pancake bunch can be estimated as follows. Suppose the bunch has a cylindrically symmetric charge density distribution $\rho(r, z)$. Assume that this can be written as the product of a surface charge density $\sigma(r)$ distribution and a longitudinal distribution function $\lambda(z)$: $\rho(r, z) = \sigma(r)\lambda(z)$. The longitudinal distribution is symmetrical in the plane $z = 0$ and is normalized to unity $\int_{-\infty}^{\infty} \lambda(z)dz = 1$, but otherwise arbitrary. To calculate the electric field at a point (r_0, z_0) inside the bunch Gauss's law is applied to a volume bounded by $0 \leq z \leq z_0$, $r_0 \leq r \leq r_0 + \Delta r$, and $0 \leq \varphi \leq 2\pi$ as depicted in figure 3.3, resulting in the following equation:

$$\pi E_z \left[(r_0 + \Delta r)^2 - r_0^2\right] + 2\pi E_r \left[(r_0 + \Delta r) - r_0\right] z_0 = \frac{2\pi}{\varepsilon_0} \int_{r_0}^{r_0 + \Delta r} r\sigma(r)dr \int_0^{z_0} \lambda(z)dz. \quad (3.9)$$

It is assumed that the z- and r-components of the electric field are slowly varying functions of r and that $\Delta r \ll r_0$. When taking terms up to the first order of Δr of the Taylor expansion of the integrand of the first integral the equation above can be simplified to:

$$E_z \left(\frac{\Delta r}{2r_0} + 1 \right) + E_r \left(\frac{z_0}{r_0} \right) \approx \frac{1}{\varepsilon_0} \sigma(r_0) \int_0^{z_0} \lambda(z) dz. \tag{3.10}$$

In the limit $\Delta r \to 0$ and assuming $\frac{E_z}{E_r} \gg \frac{z_0}{r_0}$ the following approximation holds for the longitudinal component of the electric field inside a pancake bunch:

$$E_z(r, z) \approx \frac{\sigma(r)}{\varepsilon_0} \int_0^z \lambda(r, z') dz'. \tag{3.11}$$

With equation (3.7) for an thin oblate spheroid it can be seen that the assumption $\frac{E_z}{E_r} \gg \frac{z_0}{r_0}$ is reasonable. From that equation it follows that $\frac{E_z}{E_r} \frac{r_0}{z_0} \approx \frac{A}{C}$ for a very flat oblate spheroid.

An important conclusion at this point is that E_z in a pancake bunch is proportional to the integrated longitudinal distribution and therefore independent of the detailed shape of $\lambda(z)$ [1]. As a result, an electron inside a pancake bunch experiences the same acceleration as if it were part of the ideal charge density distribution described by equation (3.8). To realize this charge density distribution the intensity profile of the laser pulse has to be shaped only transversely; the temporal shape is arbitrary. How the required pulse shape can be obtained is explained in chapter 5.

Finite creation time
Because some electrons are photoemitted earlier than others (because of a small but finite laser pulse duration) the velocities of the first electrons increase during the photoemission process. This is leading to longitudinal velocity-position correlations associated with the laser pulse duration τ_l. But the idea of the waterbag concept is that velocity-position correlations are associated with and only with the space charge field. The photoemission process can be considered as being instantaneous if the laser pulse length is much shorter than the final bunch length. The bunch length Δt due to only space charge forces at position z is given by [6]:

$$\Delta t(\gamma) = \Delta t(\infty) \sqrt{\frac{\gamma - 1}{\gamma + 1}}, \tag{3.12}$$

where Δt is expressed in terms of the Lorentz factor $\gamma = 1 + \frac{eE_{acc}z}{mc^2}$. An instantaneously created pancake bunch which is accelerated in a uniform acceleration field, expands due to space charge forces and reaches for $\gamma \gg 1$ an asymptotic length $\Delta t(\infty)$, which is given by [6]:

$$\Delta t(\infty) = \frac{mc\sigma_0}{e\varepsilon_0 E_{acc}^2}, \tag{3.13}$$

where m is the electron rest mass, c is the velocity of light, σ_0 is the surface charge density, e is the elementary charge quantum, ε_0 is the permittivity of vacuum, and E_{acc} is the strength of the uniform acceleration field. The condition that the laser pulse length has to be much shorter than the final bunch length can now be expressed as follows:

$$\tau_l \ll \Delta t(\infty) = \frac{mc\sigma_0}{e\varepsilon_0 E_{acc}^2}. \tag{3.14}$$

Image charge

The self-field or image charge field set up by emitted electrons pulls the electrons back to the cathode. This causes also undesired longitudinal velocity-position correlations. These correlations are negligible if the acceleration field E_{acc} is much stronger then the self-field $E_{self}(\sigma_0)$. This is leading to a lower limit of the acceleration field strength as a function of the surface charge density σ_0. An approximation for the self-field is $\frac{\sigma_0}{\varepsilon_0}$ [6]. This condition can then be expressed as follows:

$$\frac{\sigma_0}{\varepsilon_0} \ll E_{acc}. \tag{3.15}$$

3.3.2 Parameter space

The two conditions on the laser pulse duration and the image charge can be combined and mathematically expressed as follows:

$$\frac{eE_{acc}\tau_l}{mc} \ll \frac{\sigma_0}{\varepsilon_0 E_{acc}} \ll 1. \tag{3.16}$$

These two conditions are leading to constraints on the part of the parameter space (σ_0, E_{acc}) for which a pancake bunch will evolve into a waterbag bunch. This is named the waterbag existence regime and is visualized in figure 3.4. In this figure the laser pulse length is 30 fs. The question arises what factor should be taken for the $\ll$ symbols in equation (3.16). A first guess is a factor 10, so both $\ll$ symbols are replaced by < 0.1. This case is represented by the inner green triangle in figure 3.4. The solid black lines in figure 3.4 represent the case of equalities in equation (3.16). To find out what factor should really be taken for the $\ll$ symbols, particle tracking simulations have been done. These simulations and their results are presented in the next chapter.

According to the waterbag existence regime in figure 3.4 waterbag bunches of $1 - -10 \, \text{pC}$ can be realized with an acceleration field of 10 MV/m and an initial bunch radius of 1 mm. If these bunches can be compressed to a duration of less than 100 fs and a width of about 100 μm, then bunches have been realized, which are ideal to examine ultra-fast processes with electron diffraction. These acceleration fields can be realized relatively easily with DC photoguns. For bunches of 100 pC a higher acceleration field of about 100 MV/m is required for which RF photoguns have to be used. Waterbag bunches of more than 1 nC seem very hard to realize.

It is concluded that a pancake electron bunch with a charge density distribution $\rho(r, z) = \sigma_0 \sqrt{1 - (r/A)^2} \lambda(z)$ evolves into a waterbag bunch if the two conditions in equation (3.16) are satisfied. In the next chapter the parameter space (σ_0, E_{acc}) is explored by particle tracking simulations, and in chapter 5 it is explained how the required initial charge density distribution can be obtained.
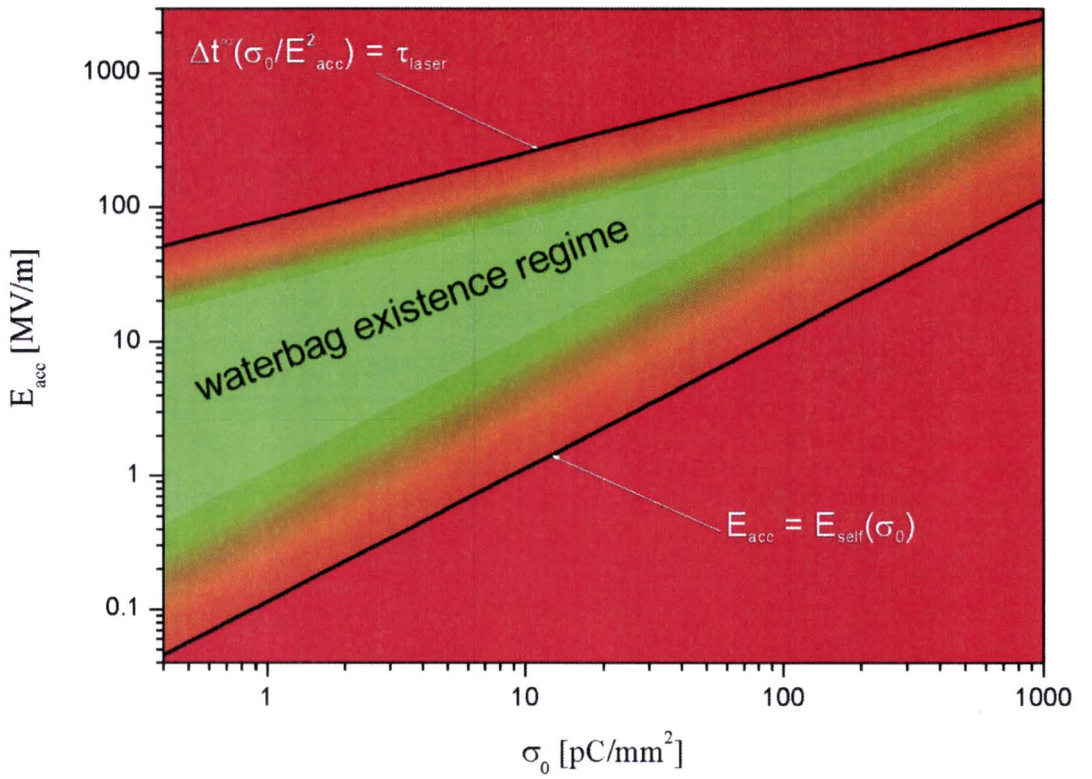
Figure 3.4: *parameter space* (σ_0, E_{acc}) *in which a pancake electron bunch will develop into a waterbag bunch if the initial charge density distribution fulfills equation (3.8). The laser pulse length is 30 fs.*

Chapter 4

Exploration of the parameter space by particle tracking simulations

In the previous chapter the waterbag existence regime is derived on the basis of simple physical, analytical arguments. In this chapter the parameter space (σ_0, E_{acc}) that follows from equation (3.16), is explored by particle tracking simulations. That is, an attempt is made to find additional support for the waterbag existence regime and to quantify the $\ll$ signs in that equation. The simulations are done with the "General Particle Tracer" code [12], GPT for short, which is briefly discussed in section 4.1.

As follows from the previous chapter a waterbag bunch has two characteristics: it is a uniformly charged ellipsoid, and it has linear position-momentum correlations. The latter is quantified by the emittance $\varepsilon_{n,x}$: the lower the emittance of a bunch, the closer to linear its position-momentum correlations are. However, a bunch with a low emittance does not necessarily have to be a waterbag. Therefor the bunch should also be a uniformly charged ellipsoid. A single criterion for this characteristic is the linearity FL of the space charge field. This quantity is introduced in section 4.2. Then results of GPT simulations for several points in the parameter space are presented and discussed in section 4.3.

4.1 GPT

GPT is a commercially available 3-D particle tracking simulation programme [12]. It is based on full 3-D particle tracking techniques, providing a solid basis for the study of charged particle dynamics in electro-magnetic fields. The relativistic equations of motion are solved by a fifth order Runge-Kutta solver. Calculations can be done with femtosecond precision. Running on a PC it can keep track of up to 10^6 interacting macroparticles. The GPT code includes:

- external fields;

- space charge fields;

- image charge fields.

Not included are retardation, field emission of electrons, and lowering of the effective work function of the cathode due to the Schottky effect.

4.2   Field linearity in a bunch

One measure for the quality of a bunch is its emittance. A low emittance is however not a sufficient condition to qualify a bunch as being a waterbag. Therefore a second parameter is required, which quantifies e.g. the linearity of the electric field inside the bunch. Generalizing on the definition of the (2-D) emittance, which quantifies the linearity of position-momentum correlations, it is proposed to define the field linearity parameter FL as follows:

$$FL \equiv \sqrt{\frac{det(\mathbf{U})}{tr(\mathbf{U})}}, \tag{4.1}$$

where $\mathbf{U}$ is a matrix which contains all correlations between position and electric field:

$$\mathbf{U} = \begin{pmatrix} <x^2> & <xy> & <xz> & <xE_x> & <xE_y> & <xE_z> \\ <xy> & <y^2> & <yz> & <yE_x> & <yE_y> & <yE_z> \\ <xz> & <yz> & <z^2> & <zE_x> & <zE_y> & <zE_z> \\ <xE_x> & <yE_x> & <zE_x> & <E_x^2> & <E_xE_y> & <E_xE_z> \\ <xE_y> & <yE_y> & <zE_y> & <E_xE_y> & <E_y^2> & <E_yE_z> \\ <xE_z> & <yE_z> & <zE_z> & <E_xE_z> & <E_yE_z> & <E_z^2> \end{pmatrix}.$$

Comparing this definition to that of the (2-D) emittance two differences are clear: the momentum is replaced by the space charge field, and the field linearity FL is normalized to the total RMS space charge field and the RMS dimensions of the bunch. With easy algebraics it can be shown that a perfect waterbag is characterized by $FL = 0$. The greater the deviation from a waterbag, the higher FL.

## 4.3   Exploration of the parameter space

A uniform acceleration field is present around the initial position of the bunch. The electrons are initiated with a radial distribution given by equation (3.8), with radius $A = 1\,\mathrm{mm}$. The bunch charge Q is represented by 10^4 macroparticles. In the simulations the electrons are ejected isotropically from the cathode surface with an energy of $0.4\,\mathrm{eV}$, resulting in a thermal emittance of $0.46\,\mathrm{mm\,mrad}$. The finite duration of the photoemission process is taken into account by initiating the particles sequentially in time, using a Gaussian temporal profile $\sim \exp(-t^2/2\sigma_t^2)$, with a full-width-at-half-maximum duration of $2.355\,\sigma_t = 30\,\mathrm{fs}$. The influence of image charges is also taken into account.

The initial bunch radius is fixed to $1\,\mathrm{mm}$, while the charge of the bunch is varied. Figures 4.1 to 4.4 show the field linearity parameter FL and the emittance $\varepsilon_{n,x}$ for bunches of 1, 10, 100, and $1000\,\mathrm{pC}$ respectively. The field linearity and the emittance are determined at $\gamma = 1.2$ (or $U \approx 100\,\mathrm{keV}$), indicated by solid, blue lines, and at $\gamma = 3.0$ (or $U \approx 1.0\,\mathrm{MeV}$), indicated by dotted, purple lines. The lines connecting the data points are only meant as a guide to the eye. In the figures the vertical black lines indicate the limits, which follow from equation (3.16) when the $\ll$ signs are replaced by equalities.

In equation (3.14) for the final bunch length $\Delta t\,(\infty)$ has been taken. For small values of γ however, the final bunch length is $\sqrt{\frac{\gamma-1}{\gamma+1}}$ times smaller, see equation (3.12). As a consequence the upper limit for E_{acc} in the parameter space is $\left(\frac{\gamma-1}{\gamma+1}\right)^{1/4}$ times lower. In figures 4.1 to
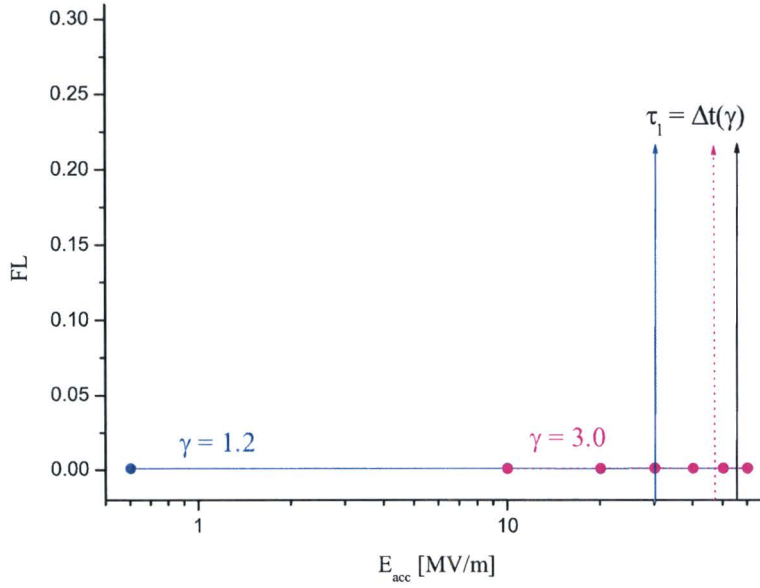
(a) field linearity
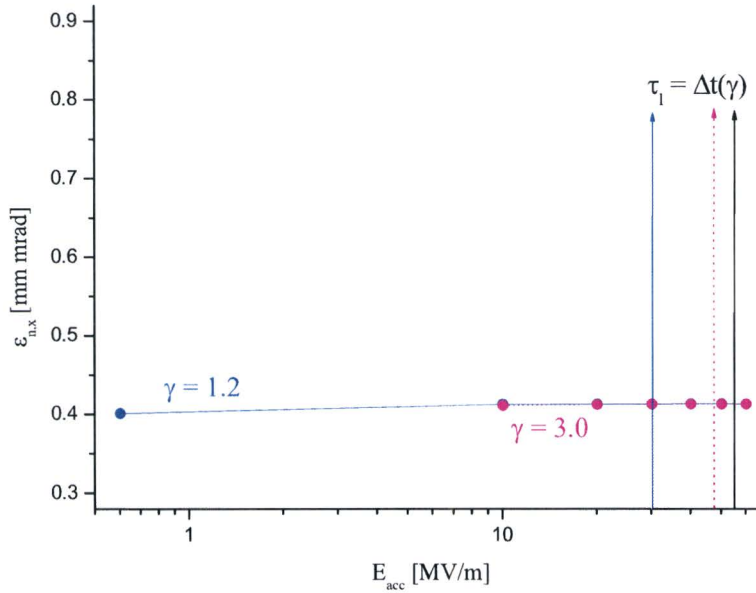
(b) emittance

Figure 4.1: *results of simulations of a* 1 pC *bunch with an initial radius of* 1 mm *and a perfect hemispheric initial surface charge density distribution, which is accelerated in a uniform electric field to* $\gamma = 1.2$ *(blue, solid line), and to* $\gamma = 3.0$ *(dashed, purple line). These lines are on top of each other. The vertical lines indicate the upper limit as they follow from equation (3.14), when the* $\ll$ *sign is replaced by an equality. The black line is for the case* $\gamma \rightarrow \infty$*, the blue line for* $\gamma = 1.2$*, and the purple line for* $\gamma = 3.0$*. The field linearity parameter (a) and the emittance (b) are shown as a function of the acceleration field strength.*
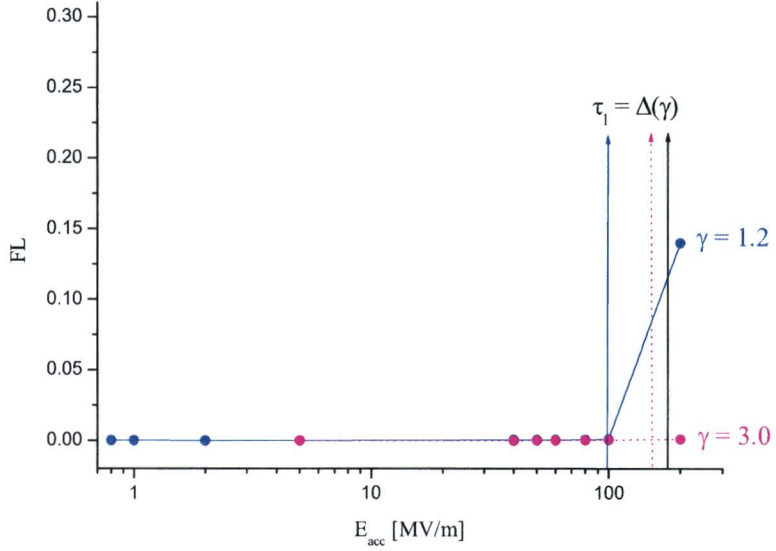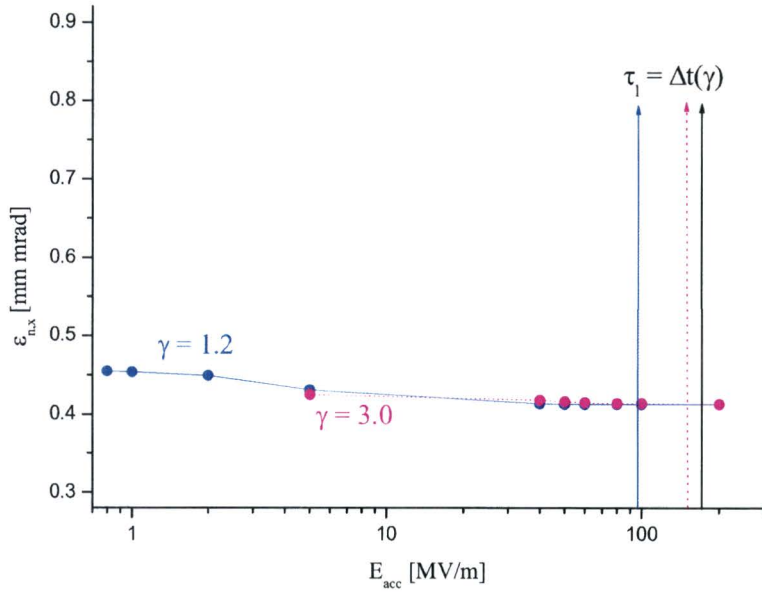
(a) field linearity

(b) emittance

Figure 4.2: *results of simulations of a* 10 pC *bunch with an initial radius of* 1 mm *and a perfect hemispheric initial surface charge density distribution, which is accelerated in a uniform electric field to* $\gamma = 1.2$ *(blue, solid line), and to* $\gamma = 3.0$ *(dashed, purple line). Parts of these lines are on top of each other. The vertical lines indicate the upper limit as they follow from equation (3.14), when the* $\ll$ *sign is replaced by an equality. The black line is for the case* $\gamma \to \infty$, *the blue line for* $\gamma = 1.2$, *and the purple line for* $\gamma = 3.0$. *The field linearity parameter (a) and the emittance (b) are shown as a function of the acceleration field strength.*

(a) field linearity

(b) emittance

Figure 4.3: *results of simulations of a* $100\,\mathrm{pC}$ *bunch with an initial radius of* $1\,\mathrm{mm}$ *and a perfect hemispheric initial surface charge density distribution, which is accelerated in a uniform electric field to* $\gamma = 1.2$ *(blue, solid line), and to* $\gamma = 3.0$ *(dashed, purple line). The vertical lines indicate the limits as they follow from equation (3.14), when the* $\ll$ *signs are replaced by equalities. The black line is for the case* $\gamma \to \infty$*, the blue line for* $\gamma = 1.2$*, and the purple line for* $\gamma = 3.0$*. The field linearity parameter (a) and the emittance (b) are shown as a function of the acceleration field strength.*
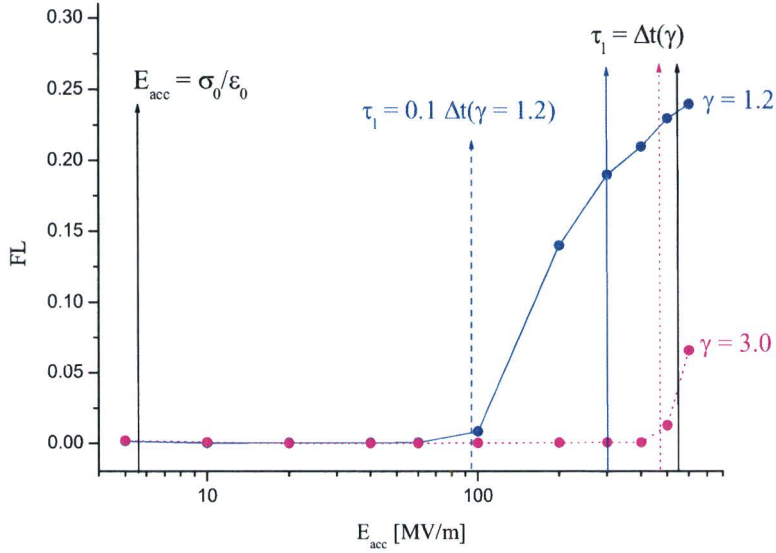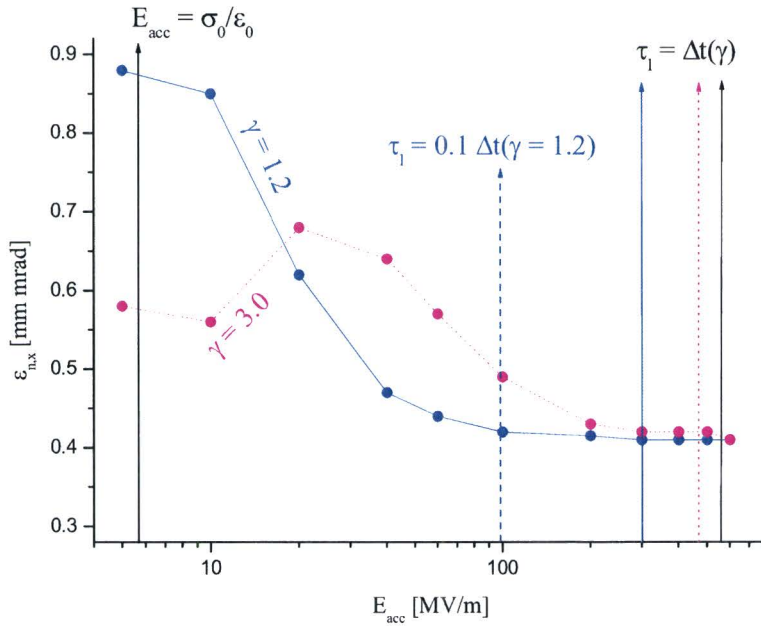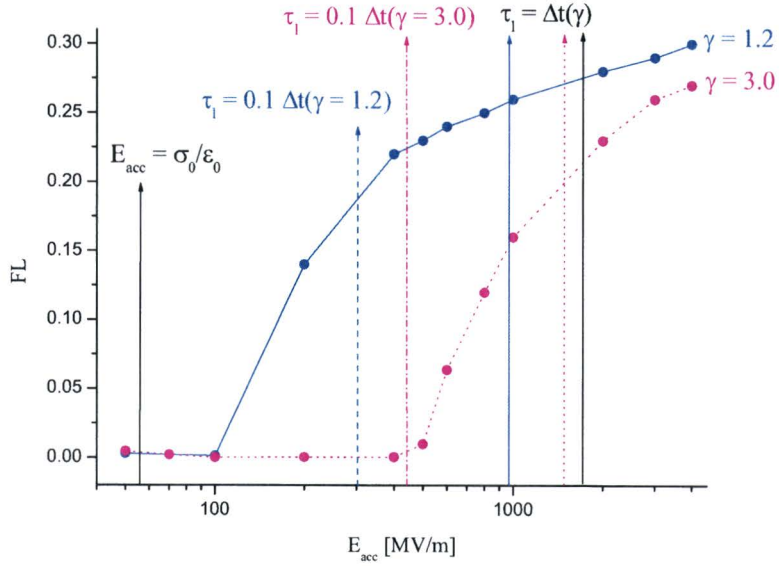
(a) field linearity
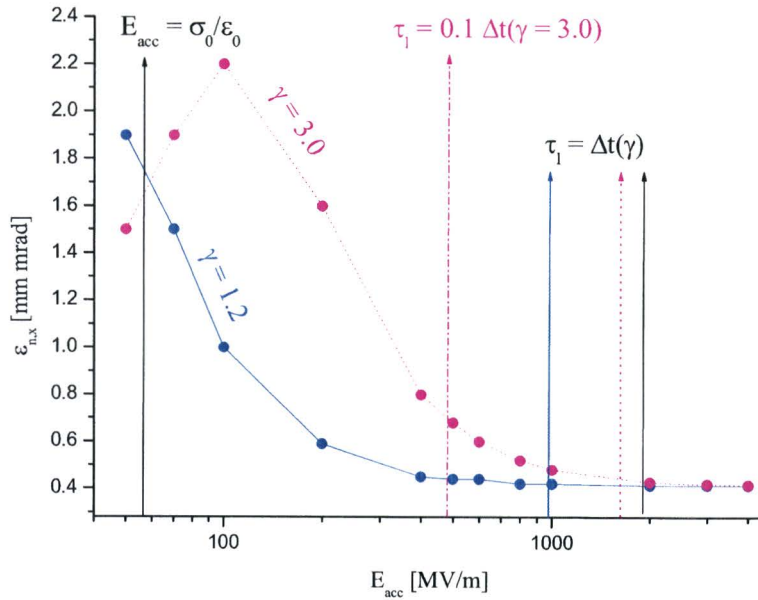
(b) emittance

Figure 4.4: *results of simulations of a* 1 nC *bunch with an initial radius of* 1 mm *and a perfect hemispheric initial surface charge density distribution, which is accelerated in a uniform electric field to* $\gamma = 1.2$ *(blue, solid line), and to* $\gamma = 3.0$ *(dashed, purple line). The vertical lines indicate the limits as they follow from equation (3.14), when the* $\ll$ *signs are replaced by equalities. The black line is for the case* $\gamma \to \infty$*, the blue line for* $\gamma = 1.2$*, and the purple line for* $\gamma = 3.0$*. The field linearity parameter (a) and the emittance (b) are shown as a function of the acceleration field strength.*

4.4 the corrected limits are visualized by a vertical solid, blue line for $\gamma = 1.2$ and a vertical dotted, purple line for $\gamma = 3.0$.

4.3.1 Discussion

For bunches of 1 and 10 pC the emittance equals the thermal emittance and the field linearity parameter is close to zero, both independently of the acceleration field strength. Only for the 10 pC bunch the corrected upper limit appears for $\gamma = 1.2$. The lower limit is not indicated in these pictures because it is only reached after the bunch has traveled such long distances, which are irrelevant in practice. Contrary to what is expected from the "traditional approach" (see section 1.3) the emittance is low when acceleration takes place in a low field. This can be explained by realizing that in these simulations the charge density is also relatively low. The development of the emittance during acceleration due to non-linear space charge forces is given by [6]:

$$\varepsilon_{n,x} = C_1 \frac{Q}{\pi \varepsilon_0 E_{acc} A} \log \left(\gamma + \sqrt{\gamma^2 - 1} \right), \tag{4.2}$$

where C_1 is a geometrical constant, which depends on the radial charge density distribution, Q is the charge of the bunch, and A is its radius. From this equation it is clear that for small charge densities the emittance remains low.

For bunches of 100 pC the upper limit shows up clearly. For $\gamma = 3.0$ it corresponds well to the theoretical limit as indicated by the vertical dotted, purple line. For $\gamma = 1.2$ the upper limit is about 3 times lower than expected, and is indicated by the vertical dashed, blue line. This factor corresponds to the first guess in section 3.3.2 of replacing the $\ll$ signs in equation (3.16) by $0.1 <$. The emittance is up to 2 times higher than the thermal emittance. For acceleration fields close to the upper limit the emittance is up to 20% higher than the thermal emittance. A reason can be that the lower limit has become relevant. The image charge field is strongly non-linear and therefore induces a relatively large emittance growth when the pancake has just been photoemitted from the cathode.

From figure 4.4 it is clear that either the emittance or the field linearity of 1 nC bunches is bad. For strong acceleration fields it is clear that the "traditional" approach as introduced in section 1.3 works to keep the emittance close to its thermal value. Regarding the field linearity upper limits of the acceleration field are clearly visible. For $\gamma = 3.0$ the upper limit is a about 3 times lower than expected, as indicated by the vertical dashed-dotted, purple line. This factor corresponds to the first guess in section 3.3.2 of replacing the $\ll$ signs in equation (3.16) by $0.1 <$. Taking the same factor for the case of $\gamma = 1.2$ results in the vertical dashed, blue line which is clearly at a too high acceleration field strength. Taking a factor 10 would be consistent with the results of the simulations.

To get an impression of the distribution in phase space figure 4.5 shows the (x, p_x) and (z, p_z) phase spaces of the 10 pC bunch at $\gamma = 3.0$, after acceleration in a uniform electric field of 40 MV/m. The phase space distributions are straight lines of finite thickness, which is due to the thermal emittance.

4.3.2 Conclusions

From these simulations it is concluded that bunches, which are ideal to examine ultra-fast processes with electron diffraction, can be realized: waterbag bunches of 1 pC and a final

energy of 100 keV can be created with an acceleration field between 0.6 and 60 MV/m. Furthermore, it is concluded that waterbag bunches with charges up to 100 pC can be created by starting out with a pancake bunch of 1 mm radius and 30 fs duration.

From the simulations it follows that the upper limit is relatively more strict for higher surface charge densities. Bunches of 1 nC with an initial radius of 1 mm can have a low emittance when being accelerated in a strong electric field, but do not evolve into waterbag bunches.

The results of the simulations are in good agreement with the analytical limits derived in the previous chapter. In order to get better insight in the correlation between the field linearity and the emittance growth, simulations without thermal emittance should be done. The definition of the field linearity parameter is just a proposal: normalization to the dimensions and/or the total space charge field might not be necessary.
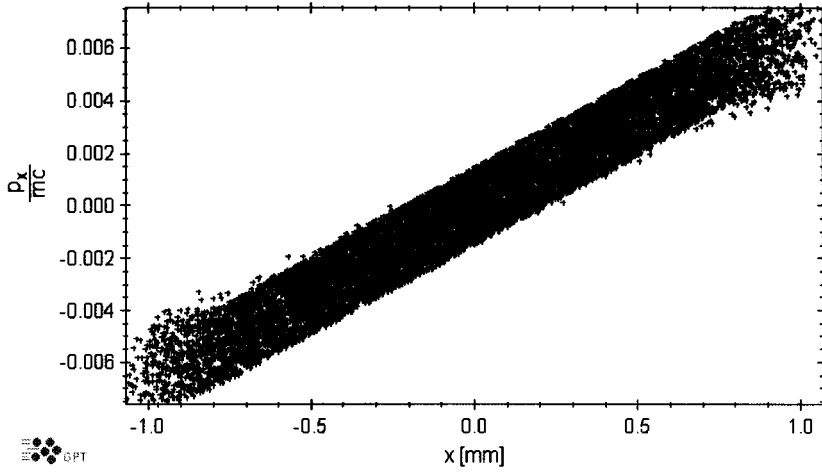
(a) (x, p_x) phase space
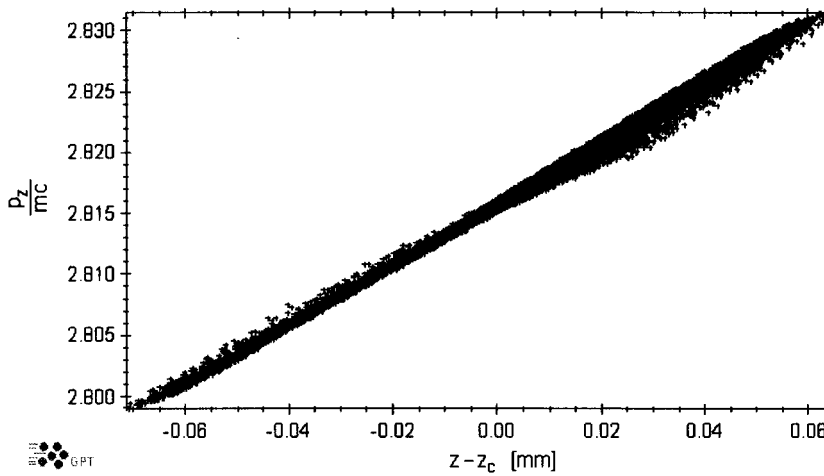
(b) (z, p_z) phase space

Figure 4.5: *results of simulations of a* 10 pC *bunch with an initial radius of* 1 mm *and a perfect hemispheric initial surface charge density distribution, which is accelerated in a uniform electric field of* 40 MV/m. *Panel (a) shows the* (x, p_x) *phase space at* $\gamma = 3.0$, *and panel (b) shows the* (z, p_z) *phase space at* $\gamma = 3.0$. *The longitudinal position* z *is relative to the center position* z_c *in the bunch.*

Chapter 5

Laser pulse shaping

For a suitable point in the parameter space (σ_0, E_{acc}) all conditions but the laser intensity profile are fulfilled and a pancake bunch evolves into a waterbag if the initial surface charge density fulfills equation (3.8). This surface charge density distribution is linked to the transverse laser intensity profile. In this chapter it is discussed how the required intensity profile can be obtained by shaping of the transverse laser intensity distribution.

First in section 5.1 the femtosecond laser system available at the TU/e is briefly discussed. In the next section the required profiles for linear and non-linear photoemission are presented. Then in section 5.3 a list of possible laser profile shapers is given. In section 5.4 it is explained how a profile shaper could best be implemented in the set-up. Finally in section 5.5 first results of laser profile shaping are presented. That is shaping of a continuous HeNe laser beam, spatial filtering of ultra-short Ti:S laser pulses (which will be used for photoemission experiments) and considerations of two possible commercially available shapers: an LCD-SLM and the piShaper. A GPT simulation with an initial charge density distribution that equals the best realized HeNe profile, is presented. Also a simulation is done with the laser intensity profile realized by the piShaper, as calculated by the manufacturer.

5.1 Available femtosecond laser system

As explained in section 3.3.1 ultra-short laser pulses are necessary to create a pancake electron bunch which will evolve into a waterbag. At the TU/e a Ti:S laser system is available which generates ultra-short laser pulses, with a minimum pulse width of 11 fs. The laser system consists of three parts: a Ti:S oscillator, a Ti:S amplifier, and a Third Harmonic Generator (THG). The oscillator generates ultra-short laser pulses of (19 ± 1) fs at a repetition frequency of 75 MHz. The center wavelength $\lambda_c = 800$ nm, and the energy per pulse is 5 nJ. At a repetition frequency of 1 kHz pulses are amplified to an energy of 1 mJ per pulse. The laser pulse length has then increased to (21 ± 1) fs. Finally the THG generates the second $(\lambda_c = 400$ mm) and third harmonic $(\lambda_c = 266$ mm). A UV pulse has an energy of maximum $100 \, \mu$J. The pulse length of both the second and third harmonic is expected to be the same as that of the fundamental pulse after the THG, i.e. (27 ± 1) fs.

5.2 Required transverse laser intensity profiles

For linear photoemission from a homogeneous photocathode the same equation holds for the transverse laser intensity profile $I(r)$ as for the required initial surface charge density distribution (equation (3.8)):

$$I(r) = I_0\sqrt{1 - (r/A)^2}. \tag{5.1}$$

This intensity distribution is referred to as "hemispheric". For non-linear photoemission processes the quantum efficiency depends on the intensity of the laser: for photoemission of order n the amount of emitted charge is proportional to the laser intensity to the power n. The resulting surface charge density distribution is thus related to the laser intensity profile by:

$$\sigma(r) \propto I^n(r). \tag{5.2}$$

For non-linear photoemission of the order n the laser intensity profile has thus to fulfill the following equation:

$$I_n = I_0 \left[1 - (r/A)^2\right]^{\frac{1}{2n}}. \tag{5.3}$$

The required intensity profiles for first, second, and third order photoemission are visualized in figure 5.1. In the limit $n \to \infty$ the required laser profile is a flat-top, which is also shown in figure 5.1. Non-linear photoemission is an interesting option for two reasons.

1. Several kinds of laser profile modulators are only available to shape red laser pulses, not UV pulses.

2. The required laser intensity profile makes that the shaping process is more efficient for non-linear than for linear photoemission. Despite the required higher intensity compared to linear photoemission, non-linear photoemission could in the end be more efficient.

In contrast to common electron bunches a waterbag bunch has sharp edges. To obtain these sharp edges a prerequisite is that the radial laser intensity profile also has sharp edges. This is indeed the case for the intensity distribution proposed, and should be kept in mind when creating the laser profile in practice.

5.3 Spatial Light Modulators

Usually the transverse intensity distribution of a laser pulse is Gaussian. In order to obtain another desired laser intensity distribution the transverse laser profile has to be shaped. Generally this can be done with a Spatial Light Modulator (SLM), which spatially modulates the amplitude and/or the phase of the electric field of the laser. All kinds of SLMs can be divided in two groups: static and dynamic. Dynamic SLMs are suitable for feedback. Because the laser profile is not perfectly stable and because of expected non-homogeneous photoemission a dynamic SLM is preferred. With feedback the SLM can be adjusted such that the initial charge density distribution fulfills equation (3.8).

Examples of dynamic SLMs are: Liquid Crystal Devices (LCD), Deformable Mirror Devices
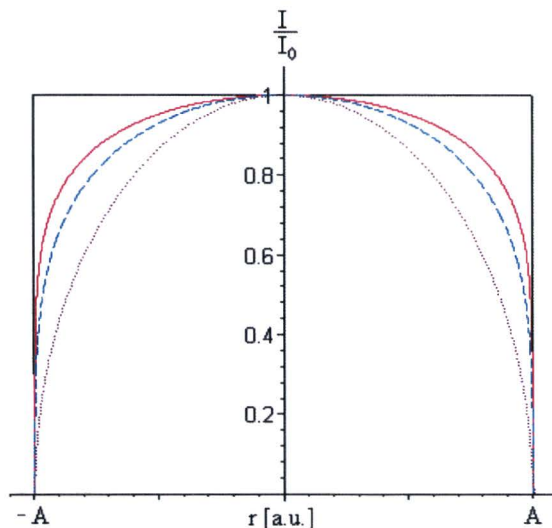
Figure 5.1: *required transverse laser intensity profiles in case of first order (dotted, purple line), second order (dashed, blue line) and third order (solid, red line) photoemission. Also a flat-top profile is shown (solid, black line). All profiles are normalized to their center intensity I_0.*

(DMD), magneto-optic SLMs, and acousto-optic SLMs. Examples of static SLMs are: microlens arrays, neutral density filters, and the piShaper [13]. Except the piShaper these SLMs are briefly discussed in reference [14]. The most suitable SLM turns out to be the SLM-LCD. However, these are not available for modulation of UV light. In that case a DMD could be used. The piShaper is discussed in section 5.5.3. It is a commercially available device and can be used for radial shaping of either UV, blue, or red laser pulses.

5.4   Laser profile shaping set-up

Two fundamentally different ways of including an SLM in the set-up have been examined [14]: shaping in the Fourier plane or in the object plane. Figure 5.2 shows schematics of these two set-ups.

Fourier plane
From Fourier optics it is known that the intensity profile in the focal plane of a lens is the Fourier transform of the intensity profile at the lens. (See e.g. reference [15] for the theory of Fourier optics.)
An advantage of shaping in the Fourier plane is that the required profiles are smooth. That is, the required profiles do not have steep edges and are therefore less demanding for the SLM. A disadvantage however is that shaping in the Fourier plane is a trade-off between efficiency and spatial resolution. To obtain at the cathode a profile with steeper edges a larger part of the Fourier transform should be created. That is, higher frequencies should be included in the created Fourier transform. Therefor the incoming laser beam should have a larger diameter. For constant laser power this has the consequence that the maximum intensity I_0 is lower.

(a) shaping in Fourier plane

(b) shaping in object plane
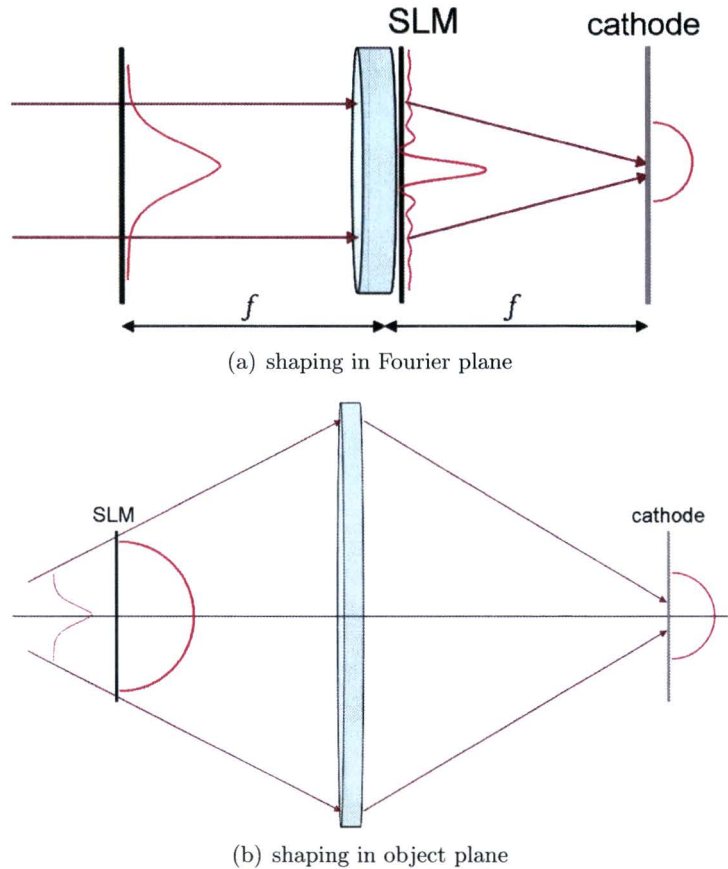
Figure 5.2: *two possible set-ups for laser profile shaping. The intensity profiles (red) are shown enlarged for clarity. (a) The SLM is placed close to a focusing lens. The incoming (Gaussian) laser beam is shaped to obtain the Fourier transform of a "hemispheric" profile. Focusing of this profile at the cathode results in the required "hemispheric" profile at the cathode. (b) The SLM is placed in the object plane. The incoming (Gaussian) laser beam is shaped to obtain the "hemispheric" profile. This profile is then imaged to the cathode.*

Object plane

Laser profile shaping in the object plane is relatively efficient and straightforward. In the object plane on the other hand, one needs to create a steep edge for which a high spatial resolution is required. It has turned out that the resolution of a LCD-SLM is high enough [14].

5.5 First results of radial laser intensity profile shaping

5.5.1 Intensity profile shaping of a HeNe laser beam

A first attempt has been made to shape the intensity profile of a continuous HeNe laser beam [14]. Different static neutral density filters have been used to shape the laser beam. The ND filters are simply slides with a fixed transmission profile. The transmission profiles have been created by printing a bitmap on the slide. The gray scale resolution of the slide is 524 pixels per cm, which is lower than the resolution of 666 pixels per cm of standard LCD-SLMs. The slide has 256 contrast steps per pixel which equals that of the LCD-SLM. The transmission functions of the filters are summarized in table 5.1 and line profiles of the corresponding shaped laser beam profiles together with the perfect hemispheric profile are shown in figure 5.3.

Table 5.1: *transmission functions of neutral density filters that are used for radial intensity profile shaping of a HeNe laser beam.*

case	transmission function
A	1 for $r < R$, 0 elsewhere
B	$\left[1 - (r/R)^2\right]^{1/2}$
C	$\left[1 - (r/R)^2\right]^{1/3}$
D	$\left[1 - (r/R)^2\right]^{1/4}$
E	$\left[1 - (r/R)^2\right]^{1/5}$
F	$\left[1 - (r/R)^2\right]^{1/6}$

Profile E in figure 5.3 resembles most the required "hemispheric" profile for generating waterbag bunches. Simulations with GPT are done for a bunch with an initial surface charge density distribution that equals profile E. The results are summarized in table 5.2. Comparing these results to that of the case of a perfect hemispheric initial surface charge density distribution, it is seen that the emittance is (almost) the same and equal to the thermal emittance. The field linearity parameter is higher but of the same order of magnitude. It is concluded that even with this non-ideal laser profile waterbag bunches can be created: the initial charge density distribution does not have to fulfill equation (3.8) exactly.

5.5.2 Spatial filtering of the femtosecond Ti:S laser pulse

The shape of the laser pulse after the amplifier is not Gaussian at all. It resembles more the TEM_{11} mode where most energy is at the edge rather than in the center of the pulse.
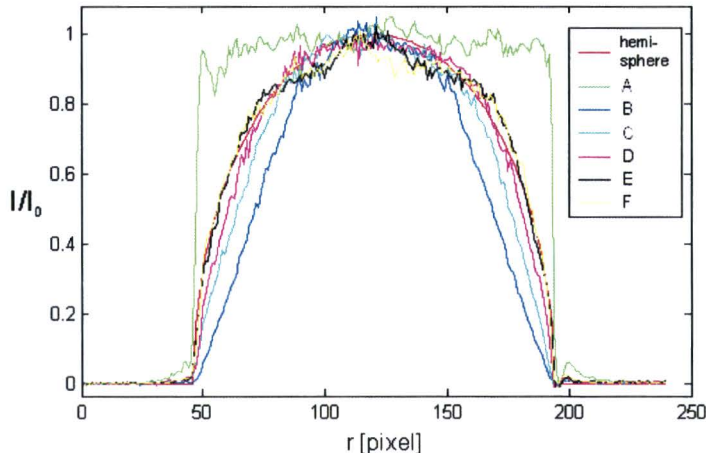
Figure 5.3: *line profiles of a HeNe laser beam after shaping with neutral density filters. The intensity I is normalized to the maximum intensity I_0. The corresponding transmission functions of the filters are summarized in table 5.1.*

Table 5.2: *results of simulations for bunches with an initial radius of* 1 mm *and an initial surface charge density distribution equal to profile E. The laser pulse has a Gaussian temporal profile with a full-width-at-half-maximum duration of* 30 fs. *The strength of the uniform acceleration field is* 10 MV/m. *Results of simulations with the ideal hemispheric initial surface charge density distribution are shown for reference.*

Q [pC]	profile	$\gamma = 1.2$		$\gamma = 3.0$	
		$\varepsilon_{n,x}$ [mm mrad]	FL [$\times 10^{-3}$]	$\varepsilon_{n,x}$ [mm mrad]	FL [$\times 10^{-3}$]
1	E	0.4	2.8	0.4	1.3
1	hemisphere	0.4	1.1	0.4	1.0
10	E	0.5	0.15	0.5	0.72
10	hemisphere	0.4	0.13	0.4	0.13

Shaping this pulse to obtain the "hemispheric" profile would be very inefficient. It would be more efficient if most energy of the pulse is in its center, like a Gaussian pulse.

With spatial filtering in principle every laser profile can be converted into a Gaussian. The principle of spatial filtering is shown in figure 5.4. A laser pulse with an arbitrary intensity profile is focussed. In the focal plane of the lens the Fourier transform of the laser pulse is obtained. As a result for every initial profile the intensity has a (local) maximum near its center at a position close to or at the focal plane. By cutting out this center peak with e.g. a pinhole, a Gaussian is obtained. The quality of this Gaussian depends on the diameter of the focused spot and of the diameter of the pinhole. In air the spot can be focused to an intensity of maximum $\sim 10^{18}$ W/m^2 before air breakdown occurs. Keeping this limit in mind the laser pulse is focussed to a diameter of 30 μm. The diameter of the pinhole is 25 μm. Figure 5.5

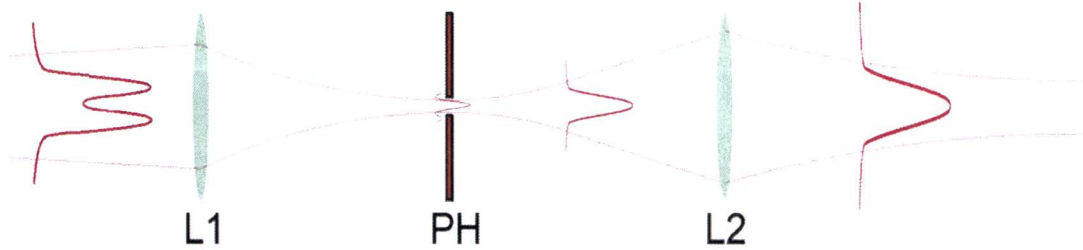L1   PH   L2

Figure 5.4: *the principle of spatial filtering. A laser pulse with an arbitrary intensity profile is focused to obtain its Fourier transform. The center peak of the Fourier transform is cut out by a pinhole, which is placed in or near the focal plane of lens 1. A second lens collimates the laser beam after the pinhole.*

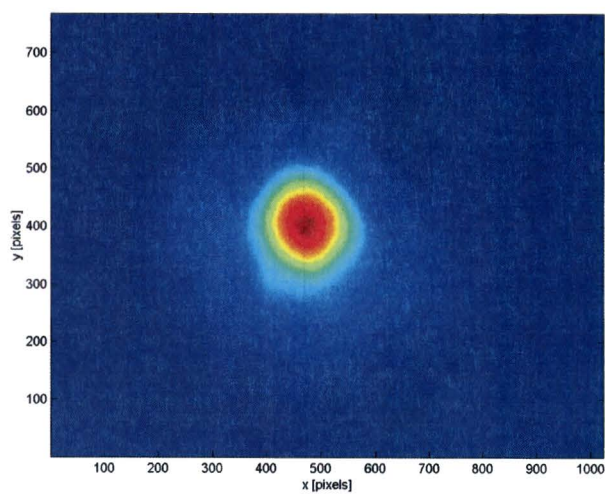shows the laser profile after being spatially filtered.

5.5.3 piShaper

The piShaper is a commercially available device which can be bought at MolTech GmbH in Germany [13]. This device has originally been developed to convert Gaussian laser profiles into flat-top profiles, but according to the manufacturer principally all kinds of profiles can be obtained. The shape of the output profile depends only on the diameter D_{in} of the input beam. The quality of the output beam depends on the quality of the Gaussian input beam. This device has been ordered recently, so it has not been used yet to shape the laser intensity profile. However, results of calculations of the manufacturer, as depicted in figure 5.6, are promising. The data of the manufacturer (black circles) are fitted to the curve $\frac{I}{I_0} = \left(1 + bx^2\right)^{-1/c}$. Comparing this equation with equations (5.1) and (5.3) gives: $A = \sqrt{-\frac{1}{b}}$ and $n = -\frac{c}{2}$. Calculations of the manufacturer for several input diameters and the results of their fits are summarized in table 5.3. It is clear that with a proper input diameter $(4.50\,\mathrm{mm} < D_{in} < 5.00\,\mathrm{mm})$ a "hemispheric" profile can be obtained.

Table 5.3: *results of fits to calculations of the manufacturer of the piShaper.*

D_{in} [mm]	A [mm]	n
5.95	flat-top	∞
5.00	2.840 ± 0.006	1.58 ± 0.02
4.50	2.880 ± 0.005	0.831 ± 0.009
4.00	2.53 ± 0.01	0.83 ± 0.03

Simulations with GPT have been done for a bunch with an initial surface charge density distribution that equals the laser profile after the piShaper in case $D_{in} = 4.50\,\mathrm{mm}$. The results are summarized in table 5.4. Comparing these results to that of the case of a perfect hemispheric initial surface charge density distribution, it is seen that the emittance is (almost) the same, i.e. practically equal to the thermal emittance. The field linearity parameter FL is higher but of the same order of magnitude. It is concluded that even with this non-ideal laser profile waterbag bunches can be created: the initial charge density distribution does not have to fulfill equation (3.8) exactly. The piShaper can be a practical device to shape the transverse

(a)
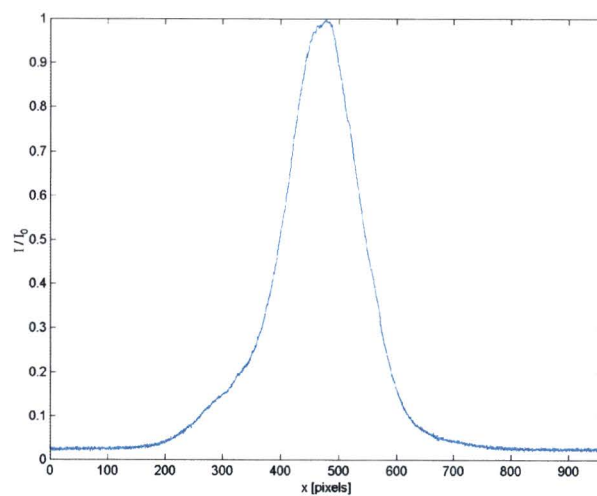
(b)

Figure 5.5: *transverse intensity profile of a Ti:S laser pulse after being spatially filtered. Panel (b) shows a line profile of the laser spot. The pixel width is 4.65 µm.*

Figure 5.6: *calculated output of the piShaper, if the input is a Gaussian laser pulse with $D_{in} = 4.50$ mm. The black dots are data points from the manufacturer's calculations. The dashed, blue line is a fit to these data points. The solid, red line is the ideal "hemispheric" profile.*

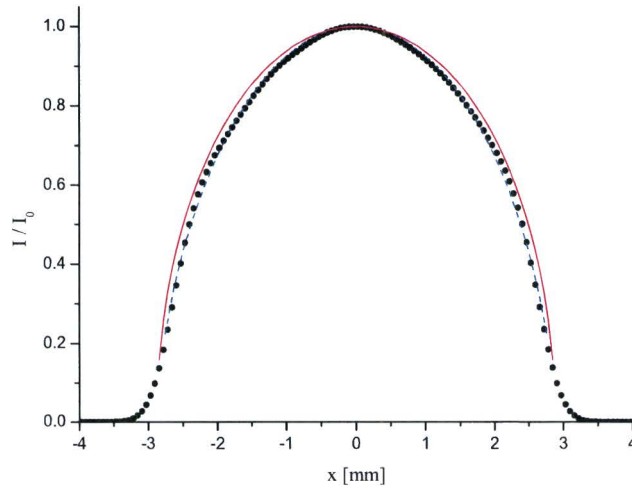Table 5.4: *results of simulations for bunches with an initial radius of 1 mm and an initial surface charge density distribution equal to the calculated profile of the laser after being shaped by the piShaper. The laser pulse has a Gaussian temporal profile with a full-width-at-half-maximum duration of 30 fs. The strength of the uniform acceleration field is 10 MV/m. Results of simulations with the ideal hemispheric initial surface charge density distribution are shown for reference.*

Q [pC]	profile	$\gamma = 1.2$		$\gamma = 3.0$	
		$\varepsilon_{n,x}$ [mm mrad]	FL [$\times 10^{-3}$]	$\varepsilon_{n,x}$ [mm mrad]	FL [$\times 10^{-3}$]
1	piShaper	0.4	2.9	0.4	1.5
1	hemisphere	0.4	1.1	0.4	1.0
10	piShaper	0.5	0.17	0.5	0.72
10	hemisphere	0.4	0.13	0.4	0.13

laser pulse intensity in order to create waterbag bunches.

A disadvantage of the piShaper is that it is a static device, so it is not possible to correct for non-homogeneous photoemission or for fluctuations in the pointing and/or the intensity distribution of the input laser beam. However, as a first step to obtain the desired "hemispheric" profile it seems a promising device.

5.5.4 SLM-LCD

An SLM-LCD seems a good device for laser beam shaping. This device is commercially available, e.g. at Boulder Non-Linear Inc. [16] and Hamamatsu [17]. The SLM-LCD is not

available for UV applications, so either red ($\lambda_c = 800$) nm or blue ($\lambda_c = 400$ nm) laser pulses should be shaped with this device. As mentioned before, this device is dynamic instead of e.g. the piShaper. With an SLM-LCD it is possible to correct for non-homogeneous photoemission and/or fluctuations in the pointing and/or the intensity distribution of the laser beam.

An important requirement is that the LCD can withstand high laser intensities. Because Boulder Non-Linear Inc. could not guarantee that the damage threshold is above $1\,\mathrm{mJ/cm^2}$ a damage test has been carried out. The result is that the damage threshold is above $2.5\,\mathrm{mJ/cm^2}$ per pulse at a repetition frequency of $1\,\mathrm{kHz}$. The laser pulse duration was 30 fs and the center wavelength was 800 nm. For detailed information on the damage test see reference [14].

Chapter 6

100 kV DC linear accelerator

To demonstrate the waterbag concept a 100 kV DC photogun has been designed and constructed. In this chapter the design is explained and results of the high voltage testing are presented. First, in section 6.1 considerations are discussed which lead to the choice for the dimensions of the accelerating structure. An overview of the entire photogun assembly is briefly presented. The photogun assembly may be split up in two parts:

1. the actual accelerating diode structure, consisting of a cathode and an anode;

2. the housing, that is the vacuum vessel enclosing the diode structure, and the high voltage feedthrough.

In section 6.2 the design of the diode is discussed in more detail. Then in section 6.3 high voltage design considerations are discussed and results of high voltage tests are presented. Next in section 6.4 the design of a solenoid (to compress bunches transversely) is discussed. In the final section possible improvements of the photogun are discussed.

6.1 Design considerations and overview

This accelerator has been designed to demonstrate the waterbag concept and to be suitable for electron diffraction. For this reason it is chosen to keep the accelerator itself as simple as possible.

As is clear from the introduction (chapter 1) for a waterbag it is not necessary to go to relativistic energies as is the case in the traditional approach, see section 1.3. Therefore a "simple" DC accelerator will serve well, and a more "complicated" pulsed DC or RF gun is not necessary. As follows from the parameter space (σ_0, E_{acc}), see figure 3.4, the acceleration field strength should be about 10 MV/m to create a waterbag with a charge of 1 pC and 1 mm initial radius. Taking into account the breakdown limit of vacuum, which is several tens of MV/m, a maximum acceleration field strength of 10 MV/m is taken as starting point. The bunch has to leave the diode through a hole in the anode. The size of this hole should be much larger than the initial pancake radius. For an initial bunch radius of 1 mm the diameter of the hole should therefore be at least 1 cm. The distortion of the acceleration field due the hole in the anode is negligible at the axis, if the distance between the cathode and the anode is larger than the radius of the hole [18]. These considerations are resulting in a 1 cm gap and a potential difference between cathode and anode of 100 kV. Power supplies of several 100 kV
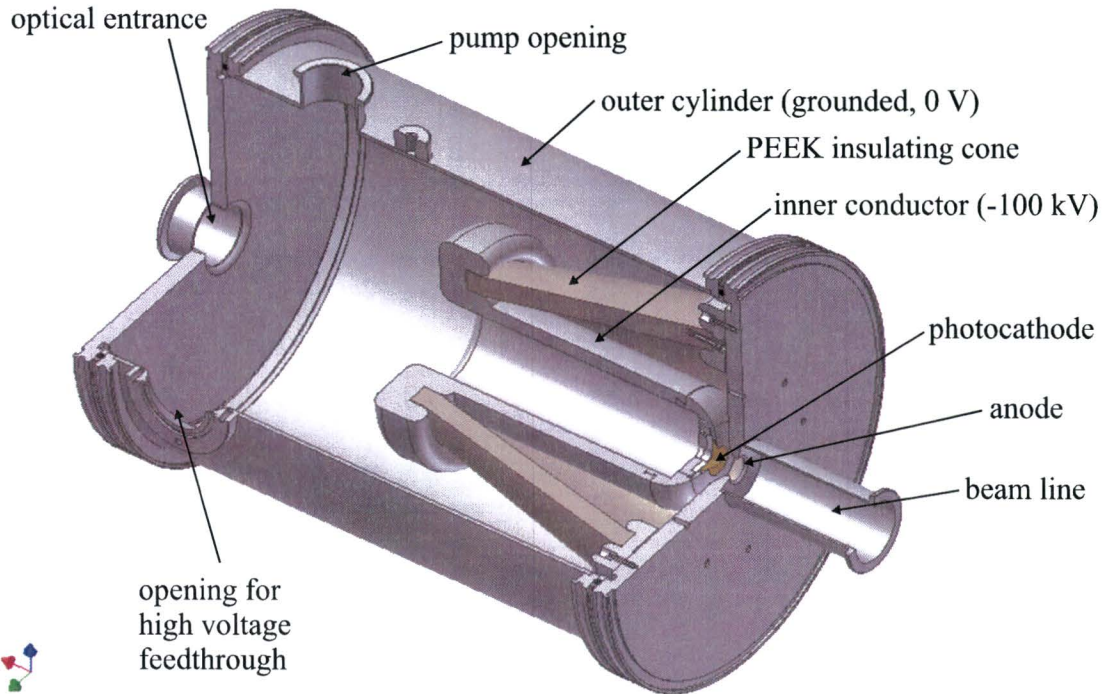
Figure 6.1: *3-dimensional view of the* 100 kV *DC photogun. The brown piece is the photocath-ode. Photoemitted electrons are accelerated towards the anode and are leaving the gun through a hole. Optical entrance for the laser beam is provided at the left side of the photogun. In this way back-illumination of the photocathode is accomplished.*

DC are commercially available. In order to keep the DC gun compact a potential difference of 100 kV (instead of e.g. 300 kV and a 3 cm gap) has been chosen.

Figure 6.1 shows an overview of the 100 kV DC photogun. The optical entrance for the laser beam is at the left side of the gun. The laser back-illuminates the photocathode (brown piece in figure 6.1). The cathode is clamped in a holder, which is screwed onto the head of a cylindrical conductor. Via the conductor a high voltage of -100 kV is supplied to the cathode. The outer cylinder, i.e. the vacuum vessel, is grounded and insulated from the inner conductor by a PEEK (PolyEtherEtherKeton) cone. The plate at the right side of the gun is the anode, which is grounded as it is connected to the outer cylinder of the gun. The photoemitted electrons are accelerated towards the anode and are leaving the gun through the hole.

All parts of the gun are made with an accuracy of 0.1 mm, which is sufficient for proper alignment of the cathode with respect to the hole in the anode.

6.2 Accelerating diode structure

The actual accelerating structure is a diode, consisting of a photocathode which is illuminated, and an anode. The photocathode is a plano-convex fused silica lens with a thin silver film on top of the convex side. Both sides of the lens are covered with an anti-reflection coating. A 1 nm thick layer of chromium is deposited on the convex side. Next a thin silver layer (of 10, 20, 30, or 40 nm thickness) is deposited, which is the actual photoemission material. These thicknesses are based on the absorption length and the electron escape length of silver as is explained in section 8.1. The chromium interlayer is to enhance adhesion of the silver film to the fused silica lens. Both the chromium and the silver are deposited by vaporization.

These kinds of cathodes can be used for back-illumination. The main advantage of back-illumination is that the paths of the laser beam and the electron beam are physically separated. When doing front-illumination the laser beam path has to make an angle with the electron beam path, resulting in a non-zero angle of incidence at the cathode. This makes the alignment of the laser path more complicated. Furthermore, the angle of incidence has to be taken into account when shaping the transverse laser intensity profile such that this profile fulfills equation (5.1) at the cathode.

A disadvantage of back-illumination is the lower yield compared to front-illumination. Also the laser damage threshold is lower, because of the thin films that are used instead of a bulk metal. This limits the maximum surface charge density of the bunch. However, it should not be a problem to create a bunch with a surface charge density of several pC/mm^2, even by third-order photoemission.

The photocathode is clamped in a holder as shown in figure 6.2. The cathode is pushed from the back to ensure electrical contact with the holder. In this way the cathode can be easily removed form the holder and replaced by another one. The photocathode can also be replaced by a bulk metal cathode (that has the same shape as the fused silica lens) to do front-illumination.
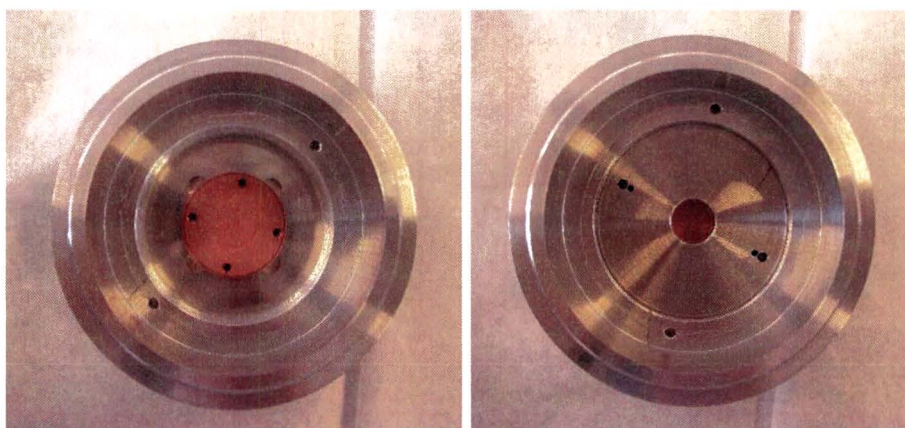

Figure 6.2: *photographs of the backside of a bulk copper photocathode clamped in the holder (left panel) and of the ring pushing at the back of the photocathode (right panel) to ensure electrical contact between the cathode and the holder.*

The diode has been carefully designed with SUPERFISH [19], a 2-D Poisson solver. Because of

the cylindrical symmetry of the geometry a 2-D solver can be used. The design of the diode is based on two requirements:

- the maximum field strength should be at the tip of the cathode;

- the acceleration field in the diode should be sufficiently uniform over the diameter of the bunch.

The first requirement ensures that the breakdown limit of the gun is determined by the diode, not by other parts of the gun. When supplying the high voltage to reach the desired acceleration field strength one does not want to be limited by other parts of the gun than the diode. The second requirement is that the acceleration field is sufficiently uniform, to prevent spherical aberrations of the electron bunch during acceleration. Simulations with **GPT** have been done to check whether the designed diode introduces any aberrations. Figure 6.3 shows a close-up of the diode structure and of the equipotential lines in the diode. Also the electric field elsewhere in the photogun has been calculated with **SUPERFISH** to be sure that everywhere in the gun the electric field is below the breakdown limit of vacuum.

(a)   (b)
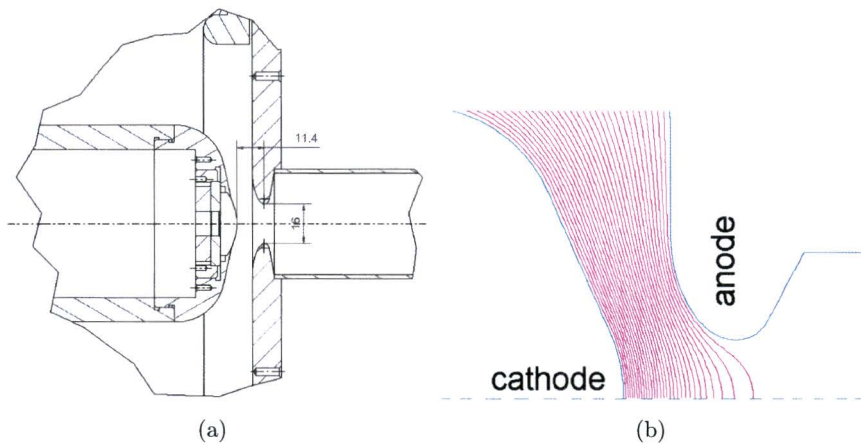
Figure 6.3: *close-up of the diode structure. In the technical drawing (a) the inner conductor, the holder, and the photocathode are clearly visible. Panel (b) shows the equipotential lines in the diode. The dashed line is the axis of symmetry.*

The shape of the cathode is that of a commercially available fused silica lens. The anode has then been optimized keeping the two requirements in mind. The ellipsoidal shape of the anode is a consequence of a trade off between rounding of the anode and distance to the cathode, such that field enhancement is maximal at the cathode's tip. The diode gap is 11.4 mm measured from the cathode's tip to the narrowest place in the anode's hole. The radius of that hole is 8.0 mm. When supplying a voltage of -100 kV to the cathode the acceleration field strength is 118 kV/cm at the cathode due to field enhancement. The effective diode gap is therefore $100\,\text{kV}/118\,\text{kV/cm} = 0.85\,\text{cm}$.

6.3   High voltage considerations

The photogun had to be designed such that if breakdown occurs, it is at the cathode's tip. Therefore understanding of breakdown mechanisms is important. In the following sections these mechanisms are discussed. In addition the 100 kV voltage supply and the high voltage feedthrough are treated.

6.3.1   Field enhancement

Consider a hemispheric bump on the surface of a flat plane in a uniform electric field. It can be calculated that the electric field is enhanced by a factor of three on the top of the hemisphere, independently on its radius. For sharp edges this factor is even higher. Therefore sharp edges have to be avoided in the photogun, so that the electric field is strongest at the cathode.

6.3.2   Vacuum breakdown mechanisms

Breakdown limits the maximum acceleration field strength and can cause irreversible damage to the acceleration structure including the photocathode. No exact theory of breakdown is known, but some mechanisms are generally accepted to (partially) describe the phenomenon. These include rest gas ionization, vaporization of whiskers, and surface tracking.

Rest gas ionization
Breakdown occurs when a *self-sustaining* current is flowing from cathode to anode. The current can be initiated by:

- thermionic emission;

- field emission;

- photoemission;

- ionization of molecules of the rest gas in the vacuum, e.g. by cosmic rays.

The released electrons are then accelerated towards the anode and are thus gaining energy. On its way to the anode an electron might collide with a rest gas molecule and ionize it, setting up an avalanche effect. Instead of ionization the electron might excite a molecule. The probability of collision depends on the pressure of the rest gas, and the probabilities of ionization and excitation depend on the energy of the electron. The ionized molecule is accelerated towards the cathode and can cause secondary electron emission. The excited molecule emits a photon when it is returning to its ground state. If this photon strikes the cathode an electron can be emitted and accelerated towards the anode. These secondary processes are leading to a series of avalanches, resulting in a self-sustaining current flow and thus in a breakdown. The breakdown voltage depends on the probabilities of collision and ionization. The energy of the electron depends on the distance traveled before collision with a molecule. So both probabilities are functions of the mean free path and thus of the pressure. The well-known Paschen law describes the breakdown voltage V_{bd} as a function of the product pd, where p is the pressure and d the distance of the gap between cathode and anode. This breakdown law is visualized in figure 6.4. For low pressures however, Paschen's law does not
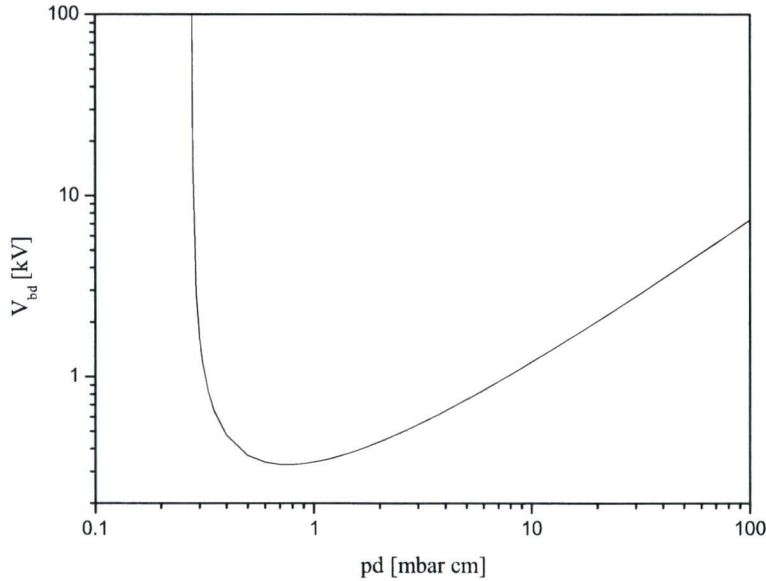
Figure 6.4: *breakdown voltage V_{bd} as a function of the product of the pressure p and the diode gap d, known as Paschen's law. For air $V_{bd,min} = 327\,V$ and $pd_{min} = 0.756\,mbar\,cm$. Figure from reference [21].*

hold anymore, because it assumes a Poisson distribution of the distance a particle travels between two subsequent collisions. According to Alston [20] for pressures below 10^{-4} mbar the mean free path of an electron is larger than about 1 m which is generally larger than the gap size. For these pressures experiments have led to the breakdown voltage as a function of the diode gap as shown in figure 6.5. According to this figure for a 1 cm gap and a potential difference of 250 kV a background pressure $p = 10^{-4}$ mbar is low enough to prevent breakdown.

Vaporization of whiskers
At low pressures, when the mean free path of an electron is larger than the gap, another mechanism is explaining breakdown: vaporization of metal, leading to a locally increased pressure. Local high current densities are present at whiskers because of field enhancement. Such a high current density can vaporize the whisker (when $E \gtrsim 2\,MV/m$ [21]) resulting in a burst of material ejected into the vacuum. In this gas pulse the collision probability is higher and breakdown can occur. The advantage however is that the whisker is now destroyed. This is also the idea of "training" or "conditioning" of an accelerator structure. By slowly increasing the voltage whiskers are vaporized and the surface is smoothed leading to a higher breakdown voltage.

Surface tracking
Another breakdown mechanism is "surface tracking", which takes place at the surface of an insulator. Also this mechanism has not been completely understood and described yet.
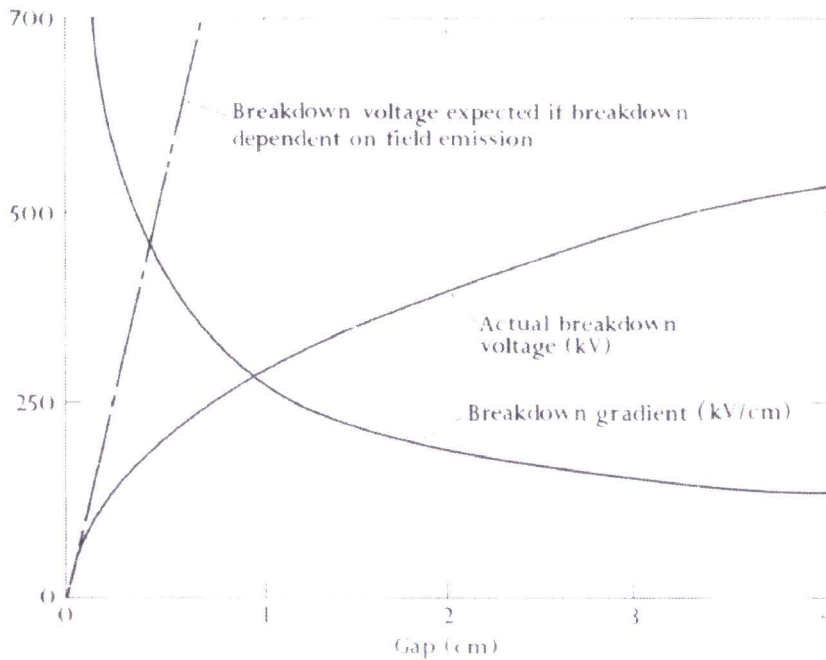
Figure 6.5: *breakdown voltage as a function of the gap width between two plane parallel electrodes in vacuum. Figure from reference [20].*

Humphries [21] gives some considerations which are helpful when designing a high voltage structure.

1. The electric field is not necessarily perpendicular to an insulator. So a released electron can be accelerated almost parallel to an insulator, gaining a lot of energy, and strike the insulator. Because of its high energy the electron may cause a burst of insulating material.

2. The secondary emission coefficient of insulators generally exceeds unity for electrons with an energy between 100 eV and a few keV. As a result impact of an (e.g. field emitted) electron is leading to a positive surface charge. This acts as an attractor for other electrons, so that the field distortion increases continuously. This non-uniform surface electric field is leading to breakdown. According to reference [22] a gradient of 3 kV/cm is safe.

To prevent mechanism 2 from happening whiskers should not be present near insulators as they can serve as an electron source as described before. Because therefore highly accurate machining is necessary, it is easier to shield the insulator ends. Figure 6.6 shows how these so-called *triple points* of metal, insulation and vacuum can be shielded.

These breakdown considerations are leading in a natural way to the dimensions of the photogun. The length of the PEEK cone should be minimum 30 cm and other distances and radii should be such that the electric field strength is lower than 100 kV/cm, except at the cathode's tip.
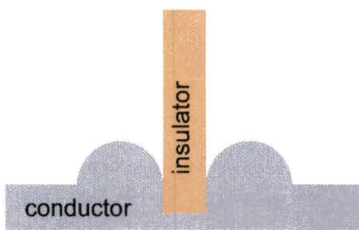
Figure 6.6: *shielding of a triple point, where insulator, conductor, and vacuum meet. The end of the insulator is shielded by a round bulge.*

6.3.3   Vacuum considerations

Although in figure 6.1 the PEEK cone seems to split the vacuum in the photogun in two parts, it is actually one vacuum. Because the electric field strength is lower outside the PEEK cone the pressure in that region could in principle be higher than inside the PEEK cone. However, then the connection of the PEEK cone to the anode should be vacuum proof and both parts should be pumped separately. Because a pressure $p = 10^{-5}$ mbar will do in both parts, it is decided to create one vacuum. The photogun is pumped from both sides with a turbopump. Outgassing of the insulating materials in the vacuum has turned out to be no problem.
The pressure of 10^{-5} mbar is also sufficient to avoid collisions of electrons in the bunch with background particles.

6.3.4   High voltage supply and feedthrough

The Matsusada [23] high voltage power supply can deliver a maximum voltage of -100 kV and maximum current of 1.5 mA. The high voltage coax cable enters the gun via a feedthrough, which is shown in figure 6.7. About 50 cm from the end of the coax cable the outer conductor is stripped off and connected to the outer cylinder of the gun. The inner conductor and the inner insulation of the cable enter the photogun. The inner conductor of the coax cable is connected to the inner conducting cylinder in the gun on which the cathode is mounted. The 50 cm of cable inside the gun is necessary to minimize surface tracking.
The inner side of the feedthrough widens exponentially. In this way the field strength is lowered along the coax cable. This so-called exponential cup is the result of a trade off between distance and rounding. A large voltage drop will now exist over the vacuum between the inner insulation of the coax cable and the feedthrough. To prevent this large voltage drop the exponential cup is filled with epoxy so that the complete voltage drops over a dielectric lowering the maximum voltage drop. Therefore it is of major concern that no air bubbles exist in the epoxy.
To prevent damage of the photocathode a 1.2 MΩ resistor can be placed between the high voltage supply and the photogun. In case of a breakdown at the cathode a current will flow to the anode. The cathode can then be seen as a charged capacitor, which is discharging in case of a breakdown. If the discharge is nearly instantaneous the cathode can be damaged because of the high current density. The resistor enlarges the RC-time in case of a breakdown so that the current density is lower. Because the coax cable is also a capacitor the resistor is placed as close as possible to the photogun. In this way the maximum charge in case of a breakdown is minimized. In case of a breakdown the high voltage mainly drops over the
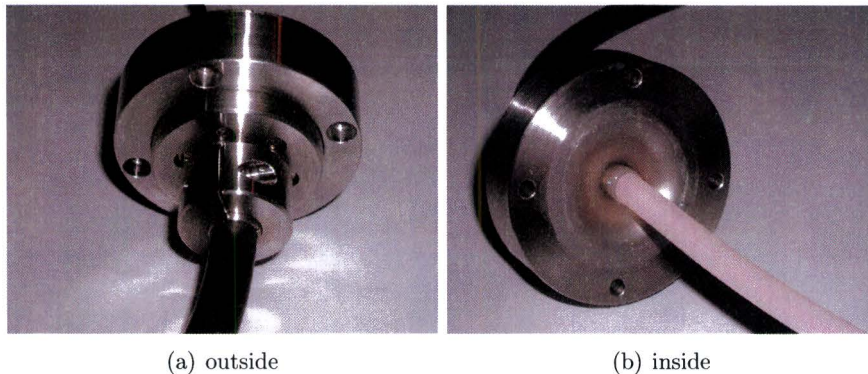
(a) outside   (b) inside

Figure 6.7: *the feedthrough of the high voltage coax cable. (a) The outer conductor of the coax cable is connected to the outer part of the feedthrough. (b) The inner conductor and the inner insulation pass through the feedthrough. The exponential cup is filled with epoxy.*

resistor. To prevent breakdown at the resistor then it is safely stored in a box filled with oil. The box is designed such that no breakdown can occur inside of it. That is, the maximum electric field strength in the box can nowhere be larger than the breakdown voltage gradient of oil.

6.3.5   Training of the 100 kV DC photogun

As explained in section 6.3.2 whiskers should be removed form the surface of the accelerator. This is done by so-called training or conditioning of the photogun. The voltage is gradually increased until breakdown occurs. The increment step is about 500 V every 2 minutes. After breakdown the voltage is increased quickly (within 1 or 2 minutes) to about 90% of the previous breakdown voltage and then gradually increased again. In this way a voltage of 73 kV has been reached without breakdown for 15 minutes.

When opening the gun the problem spot is clearly visible, see figure 6.8. It seems that the high voltage cable is too close to the wall of the outer cylinder. To solve this problem the cable has been shortened (from 50 cm to 40 cm), but still kept long enough to prevent surface tracking along the insulation of the cable. After this shortening the voltage was increased again. However, the same maximum voltage of 73 kV has been reached.

The gun has been designed for 100 kV, while in practice 73 kV is reached without breakdown. Therefore it is concluded that, considering the high voltage point, the design of the photogun is good. The maximum acceleration field is then 8.6 MV/m at the cathode, which is sufficient to create waterbag bunches with charges up to 10 pC.

6.4   Solenoidal magnetic lens

The same way optical beams can be focused by lenses, charged particle beams can be focused by magnetic fields. Magnetic elements, such as solenoids, which produce such field are therefore often called "magnetic lenses".

The focal length f of a solenoid depends on its magnetic field and on the energy of the electrons passing through it [21]:
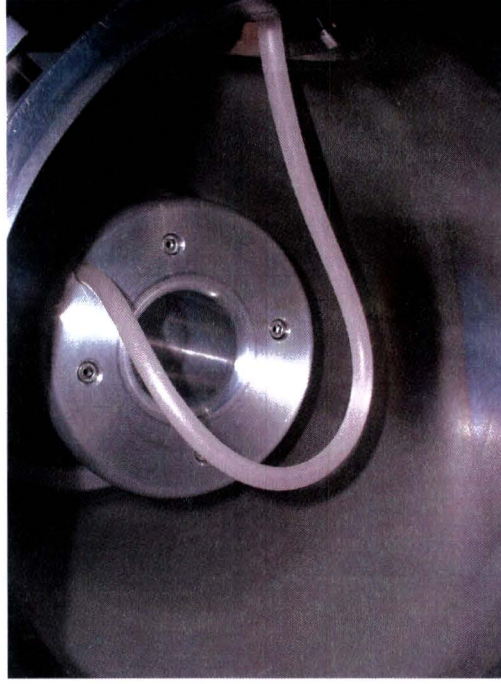
Figure 6.8: *photograph of the inside of the gun. At the right side of the cable a track is clearly visible at the vacuum vessel, which is likely due to breakdown from the cable to the wall.*

$$f = \frac{(2\gamma m \beta c)^2}{e^2 \int_0^L B_z(0,z)^2 dz},$$

(6.1)

where L is the length of the solenoid, γ is the Lorentz factor, β is the velocity of the electrons divided by the velocity of light c, and m is the electron rest mass. The z-component of the magnetic field $B(\rho, z)$ on axis of a solenoid of N loops, which is centered at $z = L/2$, is given by [24]:

$$B_z(0,z) = \frac{\mu_0 N I_s \rho_{in}}{2L(\alpha - 1)}$$

$$\left\{ \frac{z}{\rho_{in}} \ln\left[\alpha \frac{1 + \frac{1}{\alpha\rho_{in}}\sqrt{\alpha^2\rho_{in}^2 + z^2}}{1 + \frac{1}{\rho_{in}}\sqrt{\rho_{in}^2 + z^2}} \right] - \frac{z - \beta\rho_{in}}{\rho_{in}} \ln\left[\alpha \frac{1 + \frac{1}{\alpha\rho_{in}}\sqrt{\alpha^2\rho_{in}^2 + (z - \beta\rho_{in})^2}}{1 + \frac{1}{\rho_{in}}\sqrt{\rho_{in}^2 + (z - \beta\rho_{in})^2}} \right] \right\}, (6.2)$$

where I_s is the current, μ_0 is the permeability of vacuum, $\alpha = \frac{\rho_{out}}{\rho_{in}}$, $\beta = \frac{L}{\rho_{in}}$, and ρ_{in} and ρ_{out} are the inner and outer radius of the solenoid respectively. The magnetic field off-axis can be calculated using an expansion [24]:

$$B_\rho(\rho, z) = -\frac{1}{2}B_z'(0,z)\rho + \frac{1}{16}B_z'''(0,z)\rho^3 + \ldots;$$

$$B_z(\rho, z) = B_z(0,z) - \frac{1}{4}B_z''(0,z)\rho^2 + \ldots$$
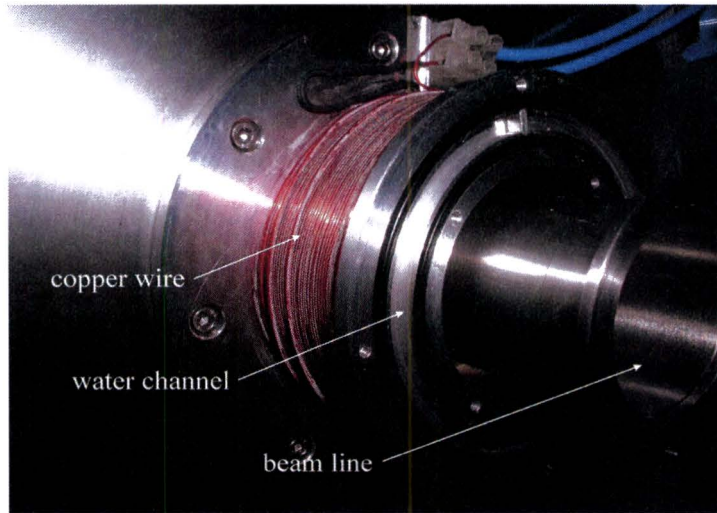
(6.3)

Figure 6.9: *photograph of the solenoid. The copper wire is red. At the right a circular channel for water cooling is visible.*

The power P dissipated by the solenoid is given by the following equation [24]:

$$P = \frac{G}{\lambda} \rho_r (NI)^2 , \qquad (6.4)$$

where $G = \frac{4}{L} \frac{\rho_{out}^2 - \rho_{in}^2}{(\rho_{out} - \rho^{in})^2}$, and ρ_r is the resistivity of the material of the wire. The fill factor λ of the solenoid is the volume of the wires divided by the total volume of the solenoid. In this way spacing between the loops is taken into account. If the power is too high the temperature of the solenoid can get above the melting point of the wire. If necessary the temperature of the solenoid can be lowered by air or water cooling.

To focus electron bunches generated by the 100 kV DC photogun a solenoid has been designed and constructed. It has $N = 600 \pm 20$ loops of copper wire of 1 mm diameter. The length of the solenoid is (42.0 ± 0.5) mm, the inner radius is (29.2 ± 0.5) mm, and the outer radius is (45.8 ± 0.5) mm. To conduct heat from the inside of the solenoid to the outside spaces between the loops are filled with thermoconductive paste. Furthermore the solenoid can be air-cooled or water-cooled. For water cooling a small circular channel is created in the side of the solenoid as shown in figure 6.9. The solenoid is placed as close as possible to the anode to compress electron bunches as soon as possible and to keep the beam line short.

The power P dissipated by the solenoid is measured as a function of the current I_s. During the measurements the solenoid was cooled by a ventilator. Figure 6.10 shows the results of the power measurements, and the theoretical graph calculated with equation (6.4) for this solenoid. The fill factor λ is taken to be $\frac{\pi}{4}$, which is the highest possible fill factor in case of wires with a circular cross-section. Air cooling of the solenoid was provided by a ventilator. For currents up to 3 A the measurements are consistent with theory. For higher currents the measured dissipated power is higher than theory predicts. In the theoretical calculation the highest possible fill factor has been taken. It is however likely that the real fill factor of the solenoid is smaller, which would lead to a smaller deviation between the measurements and
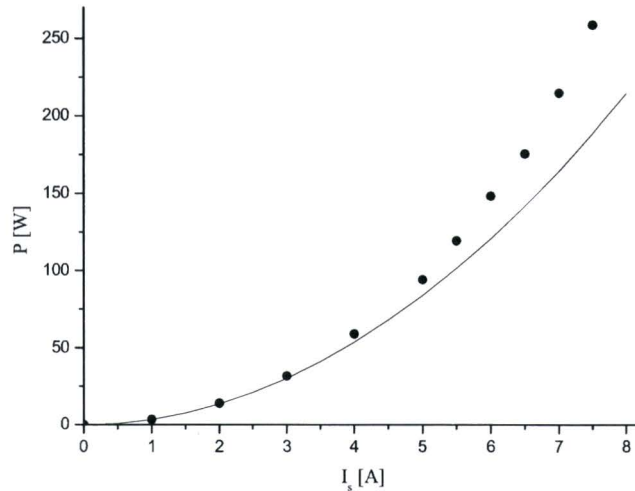
Figure 6.10: *power P dissipated by the solenoid as a function the current I_s. The dots are measurements with air cooling of the solenoid. The line is the theoretical dissipated power as given by equation (6.4).*

theory.

In case of water cooling a ventilator is still needed to blow warm air away from the solenoid. The dissipated power was the same as for the case of only air cooling. It is therefore concluded that no proper heat transfer to the water has been established.

6.5   Possible improvements

Breakdown occurs at a lower voltage than expected. A cause seems to be sparking from the high voltage cable to the wall of the outer cylinder of the photogun (see figure 6.8). Shortening of the cable to increase the distance to the wall did not solve the problem. Another solution might be a longer vacuum vessel so that the cable can be curled more parallel to the axis of symmetry rather than perpendicular to it. In this way the cable can be placed far from the wall.

A bucking coil has to be designed and created. This bucking coil is needed to null the magnetic field on the cathode surface. Without a bucking coil there is a non-zero magnetic field at the cathode resulting in an undesired initial azimuthal momentum of the photoemitted electrons. For the solenoid a thicker copper wire can be used to increase its heat capacity.

6.6   Simulation in a realistic acceleration field

In chapter 4 the waterbag existence regime was determined for uniform acceleration fields. In the 100 kV DC photogun the field is however not uniform. A GPT simulation has been done to study the development of a 10 pC bunch in the realistic acceleration field of the 100 kV DC photogun as calculated with SUPERFISH. The initial radius of the bunch is 1 mm and

the initial surface charge density distribution is perfectly hemispheric. An artificial focussing solenoid consisting of one loop, has been placed at a distance of 25 mm from the cathode surface. The solenoid current is 3000 A and the radius of the loop is 20 mm. At a distance of 15.6 cm from the cathode the bunch has an emittance $\varepsilon_{n,x} = 0.5$ mm mrad and a field linearity $FL = 0.095 \times 10^{-3}$. The emittance is almost equal to the thermal emittance, while the field linearity is slightly better than for the case of a perfect uniform acceleration field ($FL = 0.13 \times 10^{-3}$). Figure 6.11 shows the (x, p_x) and (z, p_z) phase spaces at $t = 1.0$ ns. The bunch has then traveled a distance $z = 15.6$ cm. In both phase space the distribution is a straight line of finite thickness due to the thermal emittance. It is concluded that also in the realistic non-uniform acceleration field of the 100 kV DC photogun waterbag bunches can be created.
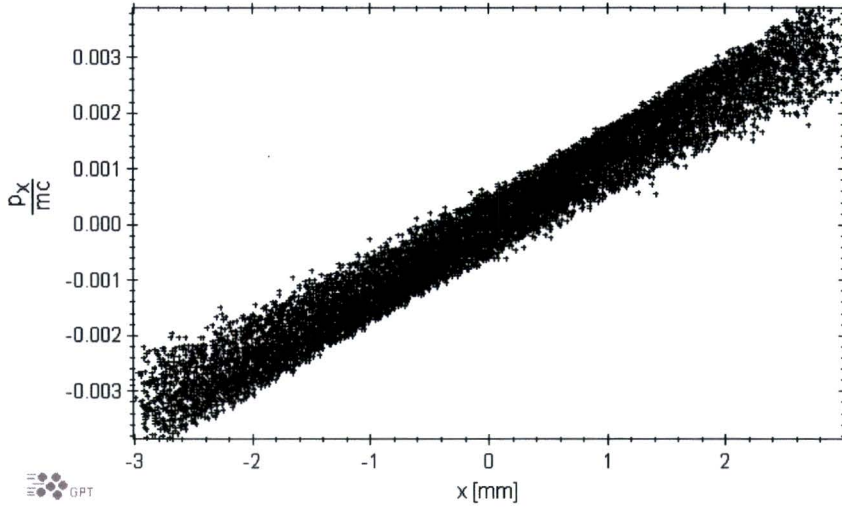
(a) (x, p_x)
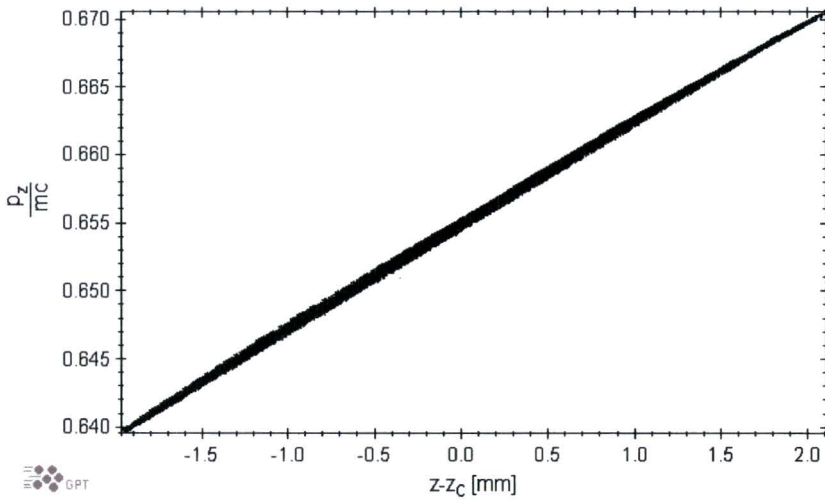
(b) (z, p_z)

Figure 6.11: *results of simulations of a* $10\,\mathrm{pC}$ *bunch with an initial radius of* $1\,\mathrm{mm}$ *and a perfect hemispheric initial surface charge density distribution, which is accelerated in the realistic electric field of the* $100\,\mathrm{kV}$ *DC photogun. (a) The* (x, p_x) *phase space at* $t = 1.0\,\mathrm{ns}$. *(b) The* (z, p_z) *phase space at* $t = 1.0\,\mathrm{ns}$. *The longitudinal position* z *is relative to the center position* z_c *in the bunch.*

Chapter 7

RF time-focusing of waterbag bunches

Creating waterbag bunches is only the first step. The next step is using its ideal properties to focus the bunch to minimum dimensions. In this chapter first in section 7.1 it is explained how waterbag bunches can be compressed longitudinally by time-dependent radio-frequency (RF) electric fields. Longitudinal compression is also referred to as time-focussing. In section 7.2 preliminary results of simulations of this focussing technique are presented.

7.1   RF time-focusing

A waterbag bunch has a positive position-momentum correlation in all directions. For time-focussing of a bunch the $(z - p_z)$-correlation has to be inverted to a negative correlation. Longitudinal compression of a bunch is in fact manipulation of its (z, p_z) phase space. For a waterbag bunch p_z is a linear function of z. To compress such a bunch the front electrons have to be slowed down relative to the center electrons, while the electrons at the back have to be accelerated. This is a rotation in (z, p_z) phase space as shown in figure 7.1. If the rotation is such that the back electrons have a higher energy than the front electrons, then the back ones will overtake the front ones. At the focal point in the beam line the bunch then has a minimum length.

The desired rotation in phase space can be realized by injection of the bunch at the proper phase of an electro-magnetic wave. This wave can be realized in practice as a standing wave in an RF cavity. The TM_{010} mode of the electric field in the cavity is given by [18]:

$$\vec{E} = E_0 J_0(kr) \sin(\omega t + \varphi_0) \vec{e}_z, \tag{7.1}$$

where E_0 is the amplitude of the electric field, J_0 is the zeroth order Bessel function of the first kind, $k = \frac{\omega}{c}$ is the wave number, $r = \sqrt{x^2 + y^2}$ the radial coordinate, and φ_0 is a phase shift. The frequency ω is given by:

$$\omega = \omega_{010} = c \frac{2.405}{R_c}, \tag{7.2}$$

where R_c is the radius of the cavity.

53
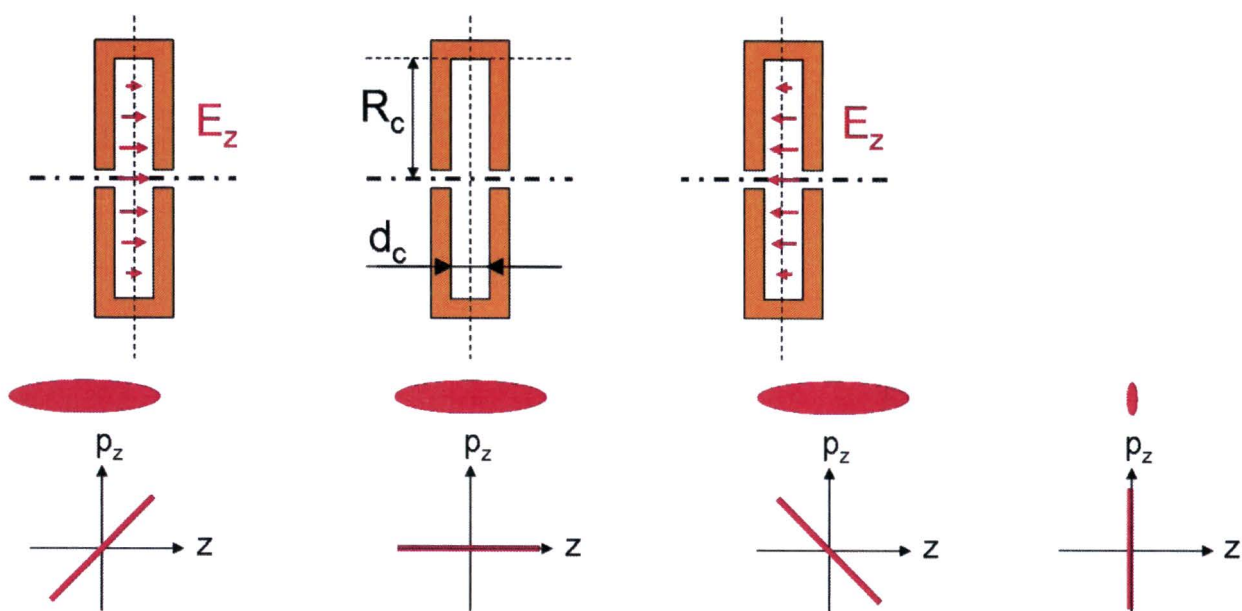
Figure 7.1: *time-focussing of a waterbag bunch with a pillbox RF cavity. If injection of the bunch takes place at the proper phase of the electric field, then the front electrons are slowed down, while the back ones are accelerated. The corresponding phase spaces are shown schematically. Time-focussing is in fact a rotation in (z, p_z) phase space. At some distance after the pillbox cavity the back electrons will overtake the front ones, resulting in an ultra-short bunch at that position.*

7.2 Simulations

Preliminary **GPT** simulations of time-focussing with a pillbox RF cavity have been done. The electric field of a realistic cavity has been calculated with **SUPERFISH** [19]. The cylindrically symmetric cavity has a radius $R_c = 38.3\,\text{mm}$, a width $d_c = 10\,\text{mm}$, and a hole with a radius of $5\,\text{mm}$ centered around the axis of symmetry. The resonant frequency of the TM_{010} mode is $3.0123\,\text{GHz}$, and the maximum field strength is $0.7\,\text{MV/m}$.

A $1\,\text{pC}$ waterbag bunch obtained by simulations with the realistic field of the $100\,\text{kV}$ DC photogun, is injected in the RF pillbox. This bunch is then time-focussed with the RF pillbox, resulting in a minimum RMS bunch length of $\sigma_t = 200\,\text{fs}$, as shown in figure 7.2. Such short bunches are ideal to study ultra-fast processes on the timescale of atomic motion by single-shot electron diffraction.

7.3 Power consumption

The required RF power P_{RF} to drive a pillbox cavity at a frequency ω_{010} is given by:

$$P_{RF} = \omega \frac{W_c}{Q_c}, \tag{7.3}$$

where W_c is the energy stored in the cavity, and Q_c is the quality factor of the cavity. An estimate for the quality factor is [18] $Q \approx \frac{2V_c}{S_c \delta_{sd}} \approx \frac{d_c}{\delta_{sd}}$, where V_c is the volume of the cavity, S_c is its total surface area, d_c is its width, and δ_{sd} is the skin depth. For a copper cavity with a resonant frequency $\omega_{010} = 3\,\text{GHz}$ the skin depth is $1.2\,\mu\text{m}$ [31]. For a cavity of $10\,\text{mm}$ width the quality factor is then $Q \approx 10^4$. The energy W_c stored in the cavity is given by [34]:

$$W_c = \frac{\pi R_c^2 d_c}{2} \varepsilon_0 E_0^2 J_1^2(2.405). \tag{7.4}$$

For the RF pillbox used in the simulations it follows that $W_c = 51.9\,\mu\text{J}$, leading to $P_{RF} = 15\,\text{W}$.
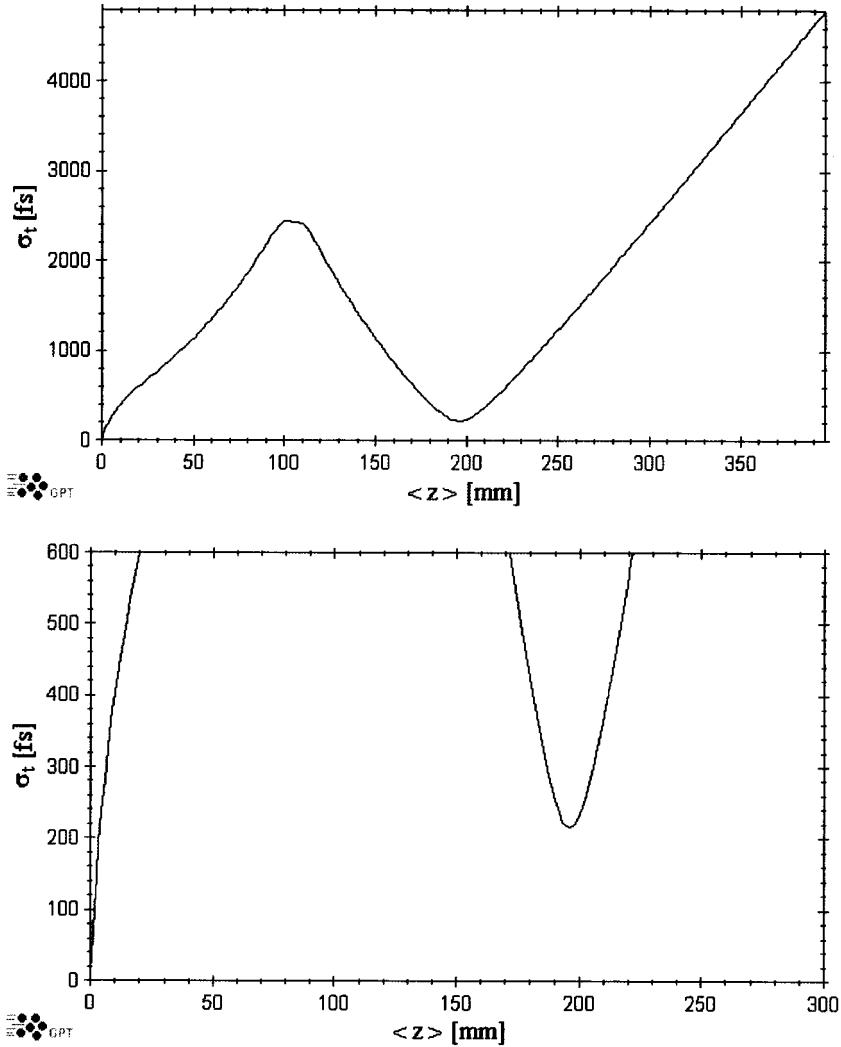
Figure 7.2: *result of a simulation of time-focussing of a* 1 pC *waterbag bunch. At* $z = 0.2$ m *a minimum RMS bunch duration of* 200 fs *is obtained. Panel (b) shows a close-up of panel (a) around* $z = 0.2$ m.

Chapter 8

Photoemission: theory and experiments

In this chapter results of photoemission measurements are presented. The experiments are done with the 100 kV DC gun which is described in chapter 6, and the laser system which is described in section 5.1. Originally the aim of the experiments was to measure the quantum efficiency of first, second, and third order photoemission by back-illumination of vacuum deposited thin silver films as a function of the laser intensity and as a function of the silver film thickness (see section 6.2). It has turned out however, that the silver film is damaged by the photoemission process, which is probably due to the chromium interlayer (see section 6.2). Other experimentalists/research groups have also observed this damage [25]. Due to lack of time new photocathodes have not been manufactured. Therefore it has been decided to do first linear photoemission by front-illumination of bulk copper. The charge of an electron bunch is measured as a function of the acceleration field strength.

In this chapter first some basic photoemission theory is explained. Then a summary of results of quantum efficiency measurements from literature is presented. Next preliminary results of the non-linear photoemission by back-illumination are presented, and finally results of linear photoemission by front-illumination.

8.1 Theory of photoemission

The photoemission process can be described by the Spicer three step model [26]:

1. optical absorption;

2. electron transport;

3. electron escape across the surface.

A light beam of intensity I is incident on a surface. Part of it is reflected, while the remainder $(1 - R)$ penetrates into the material. R is the reflectivity of the material. Inside the material light is absorbed over an absorbtion length l_α. The light intensity $I(z)$ at a distance z from the surface is thus given by:

$$I(z) = I(0)(1 - R)e^{-z/l_\alpha}. \tag{8.1}$$

The photons absorbed between z and $z + dz$ excite electrons and a fraction α_{pe} of these electrons will be excited above vacuum level. The corresponding current density J_{pe} is given by:

$$dJ_{pe} = \alpha_{pe}I(z)dz = \alpha_{pe}I(0)(1 - R)e^{-z/l_\alpha}dz. \tag{8.2}$$

Next a photoexcited electron has to travel to the surface and reach it with sufficient energy to escape. This process is governed by the escape length L_t of the material. The corresponding probability P_t is given by:

$$P_t(z) = e^{-z/L_t}. \tag{8.3}$$

For back-illumination $P_t(d - z)$ should be regarded, where d is the film thickness. With the third step, electron escape, also a probability is associated: P_e. The contribution $dJ_{pe}(z)$ to the photoemission current J_{pe} in a slab of thickness dz at a distance z from the surface is given by:

$$dJ_{pe}(z) = P_e P_t \alpha_{pe} I(z)dz, \tag{8.4}$$

leading to a photoemission current:

$$J_{pe} = I(0)(1 - R)P_e\alpha_{pe}\left[\frac{l_\alpha}{1 + \frac{l_\alpha}{L_t}}\right]. \tag{8.5}$$

Here the material is assumed to be infinitely thick. For back-illumination of a thin film of thickness d the photoemission current is given by:

$$J_{pe} = I(0)(1 - R)P_e\alpha_{pe}\left[1 - e^{-(1/l_\alpha - 1/L_t)d}\right]\left[\frac{l_\alpha}{1 - \frac{l_\alpha}{L_t}}\right]. \tag{8.6}$$

The escape length L_t is determined by the dominant scattering process, that is electron-electron scattering in metals, and electron-phonon scattering in semi-conductors. In metals a photoexcited electron loses generally so much energy in one single collision that its energy is below the vacuum level. This electron is then lost for photoemission. The escape length of a free electron in a metal is therefore equal to the electron-electron mean free path and the photoemission current is mainly due to electrons that have traveled ballistically to the surface. It is obvious that for front-illumination of a thick metal plate a material with $L_t \gg l_\alpha$ is optimum: most of the electrons are photoexcited within the escape length. For back-illumination the film thickness should not be much larger than the escape length.

All parameters in equations (8.5) and (8.6), but $I(0)$, are functions of the photon energy $\hbar\omega$. Furthermore the absorption length l_α, and the escape length L_t are also material dependent. The photoemission current is thus depending on the photon energy and on the material of the photocathode. With equation (8.5) the quantum efficiency QE of a material can be calculated. It is defined as the number of photoemitted electrons $\#_e$ per absorbed photon $\#_{ph}$:

$$QE = \frac{\#_e}{\#_{ph}} = \frac{J_{pe}/e}{I_0(1 - R)} = \frac{1}{e}\frac{\alpha_{pe}l_\alpha P_e}{1 + \frac{l_\alpha}{L_t}}. \tag{8.7}$$

For non-linear photoemission processes of the order n the photoemission current density $J_{pe,n}$ is a function of the laser intensity to the power n. This can be easily understood as follows. For higher order photoemission processes an electron has to absorb n photons in a sufficiently small time interval dt. The probability that an electron absorbs a photon in a time-interval dt is proportional to the number of photons $\#_{ph}$ that are present in the direct surrounding of the electron in that time-interval. The probability that an electron absorbs a second photon is proportional to $\#_{ph} - 1$, and so on for higher orders. So the probability that an electron absorbs two photons in a time dt is proportional to $\#_{ph}(\#_{ph} - 1) \approx \#_{ph}^2$. The number of photons per unit time and per unit area is of course given by the laser intensity. So it is concluded that $J_{pe,n} \propto I^n$. The total current density can then be described by the combined effect of all n partial contributions, that is thermionic emission, one-photon emission, and multi-photon emission (or non-linear photoemission). This description is called the BSB-model, named after Bechtel, Smith, and Bloembergen [27] and is expressed by the following equation:

$$J_{pe,tot} = \sum_{n=0}^{\infty} J_{pe,n},\tag{8.8}$$

where $J_{pe,tot}$ is the total photoemitted current density, and n is the order of the photoemission process. The current density $J_{pe,n}$ is the partial current density associated with the photoemission process of the order n. For each order the following general expression holds [27]:

$$J_{pe,n} = a_n \left(\frac{e}{\hbar\omega}\right)^n A I^n (1 - R)^n T^2 F\left(\frac{n\hbar\omega - \Phi_e}{k_B T}\right) = b_n I^n,\tag{8.9}$$

where e is the elementary charge, $\hbar\omega$ is the photon energy, A is the theoretical Richardson coefficient, I is the incident laser intensity, R is the surface reflectivity, T is the absolute temperature of the surface, k_B is Boltzmann's constant, and Φ_e is the effective surface work function. The constant a_n contains the electron escape probability and the n-photon absorption coefficient. This constant has to be determined experimentally. The constant b_n is often called "non-linear constant". The Fowler function F is given by [28]:

$$F(x) = \begin{cases} \sum_{k=1}^{\infty} (-1)^{k+1} \frac{e^{kx}}{k^2} & , x \leq 0 \\ \frac{\pi^2}{6} + \frac{x^2}{2} - \sum_{k=1}^{\infty} (-1)^{k+1} \frac{e^{-kx}}{k^2} & , x \geq 0. \end{cases}\tag{8.10}$$

8.2 Quantum efficiencies from literature

In literature several results of quantum efficiency measurements are published for both front- and back-illumination. For back-illumination only quantum efficiency measurements of *linear* photoemission have been found. Table 8.1 summarizes several values of the non-linear constant b_n and of the quantum efficiency QE as found in reference [29]. For non-linear photoemission QE is not given, because it is a function of the incident light intensity. In reference [29] also the ratio $\frac{back}{front}$ as a function of the film thickness d (for back-illumination) is presented. Fitting of those data leads to the following equation:

$$\frac{back}{front} = e^{\alpha_{bf}d}, \tag{8.11}$$

with $\alpha_{bf} = (-5.1 \pm 0.1) \times 10^7 \, \text{m}^{-1}$. The measurements in this reference are all done with a copper cathode. The material properties (absorption length, escape length and work function) of copper and silver are comparable, so that the order of magnitude of the quantum efficiency and of the non-linear constant are equal.

Table 8.1: *non-linear constant b_n and quantum efficiencies for front-illumination [29].*

n	λ [nm]	b_n [(pC/m^{2}s)/(W/m^2)^n]	QE
1	266	$(2.1 \pm 0.1) \, 10^6$	$(1.0 \pm 0.1) \, 10^{-5}$
1	217	$(1.9 \pm 0.1) \, 10^8$	$(1.1 \pm 0.1) \, 10^{-3}$
2	325	$(6.6 \pm 0.6) \, 10^{-7}$	
3	650	$(5 \pm 1) \, 10^{-23}$	

In reference [30] it is shown that the quantum efficiency strongly depends on the wavelength of the laser and on the cleaning of the photocathode. For illumination of copper with 266 nm laser pulses quantum efficiencies of up to 10^{-4} are possible.

8.3 Experiments

8.3.1 Aim

The aim of the experiments is to measure the yield of first, second, and third order photoemission by back-illumination of a silver cathode and to do this for different thicknesses of the silver film. For silver the escape length $L_t = 6 \, \text{nm}$ [26]. For thicker films the electron yield should thus decrease. To study this effect film thicknesses of 10, 20, 30, and 40 nm are used. A second goal is to do front-illumination on a copper bulk cathode (which has the same shape as the cathodes for back-illumination, see section 6.2). In this experiment the maximum possible photoemitted charge as a function of the acceleration field is determined.

8.3.2 Set-up

The quantum efficiencies of non-linear photoemission by back-illumination have been measured with the photogun described in chapter 6. Figure 8.1 shows a schematic of the diode, the beam line, and the laser paths for both back- and front-illumination. A femtosecond laser (see section 5.1) illuminates the back-side of a silver cathode. (See section 6.2 for a detailed description of the cathode). This silver film is so thin, that electrons will be emitted at its front-side. These emitted electrons are accelerated towards the anode and leave the diode through a hole in the anode. The electrons are captured in a Faraday cup. For a detailed description of the Faraday cup see reference [31]. As a result of space charge the electron bunch grows transversely. A consequence could be that the bunch diameter is larger than the iris of the Faraday cup. In order to capture all the electrons in the cup the bunch is focused transversely by a solenoid (see section 6.4). The signal of the Faraday cup is buffered by a Canberra 2004 pre-amplifier and then, if necessary, shaped and amplified by an Ortec 372 shaping amplifier. The shaping time equals 1 μs and the gain equals 20. In the end the signal is read out with an oscilloscope. The Canberra pre-amplifier has a test-input which
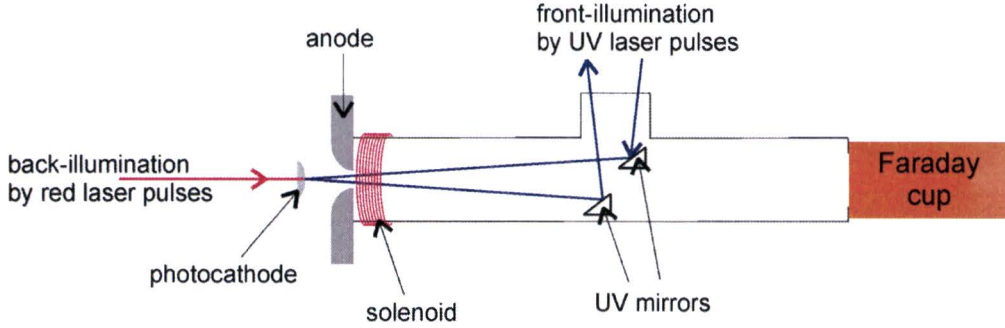
Figure 8.1: *schematic of complete set-up for quantum efficiency measurements.*

is used for calibration. The output voltage of the combination of pre-amplifier and shaping amplifier is very sensitive to the supplied voltage. When calibrating this amplification set-up even a small uncertainty in the supplied voltage results in a relatively large uncertainty in the calibration factor. As a result the uncertainty in the measured charge is also relatively large. For front-illumination a bulk copper cathode is used. This cathode has the same shape as the fused silica lenses on which the silver films are deposited for back-illumination. The laser beam enters from the side of the electron beam line and travels via a mirror to the cathode. The reflection from the cathode travels to another mirror and leaves the beam line. This is shown schematically in figure 8.1. The electron bunches have to pass through the gap between these two mirrors to be captured in the Faraday cup. (In case of back-illumination these UV mirrors are removed.)

The intensity distribution and the size of the laser spot are measured with a Sony X710 CCD camera. From this picture the area of laser spot is determined. Also the non-linear constant b_n is determined by summation over the pixel values to the power n:

$$b_n = \frac{Q}{A_p \tau_l} \frac{1}{\sum\limits_{i=1}^{N_r} \sum\limits_{j=1}^{N_c} I_{ij}^n},$$

where A_p is the area of a pixel, Q is the charge of the bunch, and τ_l is the laser pulse duration. The laser spot covers an area on the CCD capture that is given by N_r rows and N_c columns.

8.3.3 Third order photoemission by back-illumination

Red ($\lambda_c = 800\,\mathrm{nm}$) laser pulses are used for back-illumination of thin silver films. These cathodes are described in section 6.2. The (average) laser power is $(25 \pm 1)\,\mathrm{mW}$ at a repetition frequency of $1\,\mathrm{kHz}$. The laser pulse length is approximately $35\,\mathrm{fs}$, according to reference [31]. Combining these numbers leads to an energy $E_p = (25 \pm 1)\,\mu\mathrm{J}$ per pulse and a peak power of $0.71\,\mathrm{GW}$. The intensity profile of the laser is measured with a CCD camera to determine the spotsize. Figure 8.3 shows a CCD capture of the laser spot. From that figure the non-linear constant $b_3 = J_3/I^3$ is calculated as explained in the previous section.

For the silver film of $30\,\mathrm{nm}$ thickness two quantum efficiency measurements are done at different laser intensities. To determine the charge of a bunch an average of 512 bunches is taken. The signal of the Faraday cup is measured with the shaping amplifier. For each measurement the laser pointing and the solenoid current are adjusted such that charge collected by the

Faraday cup is maximum. The results are summarized in table 8.2.

Table 8.2: *results of third order QE measurements.*

$<I>$ [GW/cm^2]	Q [pC]	b_3 [(pC/m^{2}s)/(W/m^2)^3]	QE
70	0.6 ± 0.2	$(1.2 \pm 0.4)\ 10^{-24}$	$(6 \pm 2)\ 10^{-9}$
186	0.4 ± 0.2	$(0.5 \pm 0.2)\ 10^{-24}$	$(4 \pm 2)\ 10^{-9}$

First it should be concluded that with this laser system bunches of 1 pC can be created by back-illumination of thin silver films. Therefor the laser power should be increased, which can be done up to 1 mJ per pulse. That is 40 times higher than the laser power in this experiment. Furthermore it is likely that the measured charge is lower than it really was due to ballistic deficit. This effect has been observed for experiments of linear photoemission by front-illumination and is explained in section 8.3.4.

Contrary to what is expected the charge is lower at a higher laser intensity. When examining the photocathode after the experiments it is clear that the silver film has been damaged. In figure 8.2 a clear line is visible corresponding to a sweep of the laser pointing. At this line there is no or little silver visible. The width of the line is about 0.2 mm, which is half of the FWHM width of the laser spot. This kind of damage only happens when the acceleration field is non-zero, so it can not be caused by too high laser intensities. Other experimentalists/research groups have observed the same [25]. Their experience is that the chromium interlayer (see section 6.2) plays an important role: without this chromium layer the photocathode does not get damaged. It is therefore recommended to create new photocathodes without an interlayer and to do the back-illumination experiments again. To increase adhesion at the rim of the photocathode, where it is clamped in the holder, first chromium could be deposited by using a mask. Another option is to use copper instead of silver.

The non-linear constant b_3 is calculated directly from the CCD capture. First the value of every pixel is raised to the power three, then these values are summed to calculate b_3. The values thus obtained are almost two orders of magnitude smaller than that from reference [29]. First it should be noticed that in reference [29] b_3 is measured for front-illumination, while in this report photoemission by back-illumination is done. This accounts only for a factor 5. The difference is then however still an order of magnitude. An explanation could be that the intensity to the power three as calculated from reference [29] is calculated as $<I>^3$. That is averaging the intensity followed by raising to the power three. The non-linear constants resulting from the measurements in this report are calculated by using $<I^3>$, that is first raising to the power three (per pixel) followed by averaging. It can be shown easily that $<I>^3 \leq <I^3>$. As a consequence b_3 is higher when using $<I>^3$ instead of $<I^3>$. The amount of discrepancy depends on the intensity distribution of the laser, which is not given in reference [29].

In reference [32] the charge is measured as a function of the intensity. Because the spotsize is not given b_3 can not be calculated. To compare the results of this report with those in reference [32] the ratio $\frac{Q}{<I>^3}$ is calculated. For the measurements in this report $\frac{Q}{<I>^3}$ equals 1.8×10^{-45} pC/(Wm^{-2})^3 and 6.2×10^{-47} pC/(Wm^{-2})^3 respectively. In reference [32] this ratio equals 6.5×10^{-45} pC/(Wm^{-2})^3. The order of magnitude of $\frac{Q}{<I>^3}$ of the first measurement is thus consistent with literature. The results of the second measurement is inconsistent, because of the damaged photocathode. This discrepancy in the two measurements is also clear when examining the non-linear factor b_3, which is one order of magnitude smaller for

Figure 8.2: *microscope image of the line on a damaged photocathode. At this line the transparency of the cathode is higher than at the unaffected part. No or little silver is visible at this line. The width of the line is about 0.2 mm.*
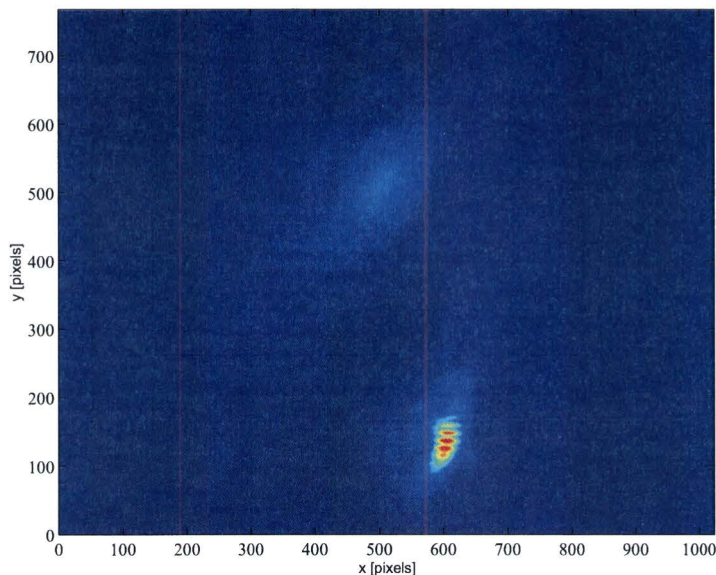

Figure 8.3: *CCD capture of a cross-section of the UV laser pulse. Two spots are clearly visible, one brighter than the other. The pixel width is 4.65 μm.*

the second measurement. The quantum efficiency has not dropped significantly, but this is because it is a function of the laser intensity.

8.3.4 Linear photoemission by front-illumination

Ultra-violet ($\lambda_c = 266$ nm) laser pulses are used for photoemission of electrons from a bulk copper cathode. The average power is (32 ± 2) mW at a repetition frequency of 1 kHz. The laser pulse length is approximately 50 fs [31]. Combining these numbers leads to an energy $E_p = (32 \pm 2)\,\mu$J per pulse and a peak power of 0.64 GW.

Figure 8.3 shows a CCD capture of the UV laser spot. In fact two spots are visible, one brighter than the other. The distance between the centers of these spots is 1.6 mm. This distance is so small that it would be likely that the photoemission current from both spots is focused into the Faraday cup. The FWHM widths of the spots are 0.44 mm (weak spot) and

0.18 mm (bright spot), leading to a photoemission area with a diameter $d = 2.2$ mm. The average intensity is then $< I >= \frac{E_p}{\tau_l \pi d^2/4} = 1.68 \times 10^{14}$ W/m^2.

From the CCD capture the intensity of both spots is determined: $I = 9.2 \times 10^{14}$ W/m^2 for the weak spot, and $I = 3.9 \times 10^{15}$ W/m^2 for the bright spot. The intensity of the bright spot is thus only 4 times higher than that of the weak spot. The contribution of the weak spot to the photoemission current should therefore not be neglected.

The total photoemitted charge is measured as a function of the acceleration field. The acceleration field is varied from 10 kV/cm to 50 kV/cm in steps of 2.5 kV/cm. At each measurement the laser pointing and the solenoid current are adjusted such that charge collected by the Faraday cup is maximum. To determine the charge of a bunch an average of 512 bunches is taken. Figure 8.4 shows the results of the measurements of the charge Q as function of the acceleration field E_{acc}. First it is concluded that by UV front-illumination of bulk copper bunches of more than 10 pC can be created.

For the highest measured charge the quantum efficiency and the factor b_1 (see equation (8.9), calculated directly from the CCD capture) are determined: $QE = (2.0 \pm 0.1) \times 10^{-6}$ and $b_1 = 1.3 \times 10^6$ (pC/m^{2}s)/(W/m^2)). The quantum efficiency is one order of magnitude smaller than the one in literature, whereas b_1 is of the same order of magnitude (see table 8.1). This can be explained by misalignment so that not all charge has been detected. The UV laser spot actually consists of two spots. It is likely that the contribution to the photoemitted charge of one spot is not or not completely focused into the Faraday cup. To calculate the constant b_1 the laser intensity is determined from the CCD capture of the UV laser spot, not from a direct laser power measurement. Therefore QE can be inconsistent with b_1.

From figure 8.4 it is clear that the charge is an increasing function of the acceleration field strength. A reason could be that the charge density of the photoemitted bunch is so high that its space charge field cancels the acceleration field near the cathode surface. If now more electrons would be photoemitted, then the space charge field would be higher leading to an electric field which pushes the electrons back into the cathode. So the photoemission process is *space charge limited*. In figure 8.4 the space charge limited regime is above the line $Q = \varepsilon_0 \pi R^2 E_{acc}$, where R is the initial radius of the bunch. For non-relativistic energies and continuous beams the maximum current density in the space charge limited regime is described by Child's law [33]:

$$J_{pe} = \frac{4\varepsilon_0}{9} \sqrt{\frac{2e}{m}} \frac{V_{acc}^{3/2}}{d^2}, \qquad (8.12)$$

where J_{pe} is the current density, V_{acc} is the potential difference across the diode, and d is the diode gap.

Next it is clear in figure 8.4 that the measurements with the shaping amplifier are inconsistent with those without the shaping amplifier. A cause could be so-called ballistic deficit: the shaping time is shorter than the length of the input signal. As a result only the first part of the input signal is shaped and amplified. This is leading to a lower signal than it should be. That is also what can be seen in figure 8.4: the charge determined with the shaping amplifier is lower than the charge determined without the shaping amplifier. With Child's law the bunch length can be calculated as follows. For the diode used in this experiment $J_{pe} = V_{acc}^{3/2} \times 0.0364$ AV$^{-3/2}$m^{-2}. Figure 8.4 shows also a fit of the data to the curve $Q = a_{cl}V_{acc}^{3/2}$. The result is $a_{cl} = (0.045 \pm 0.002)$ pC/V$^{3/2}$. When the cross-section A of the
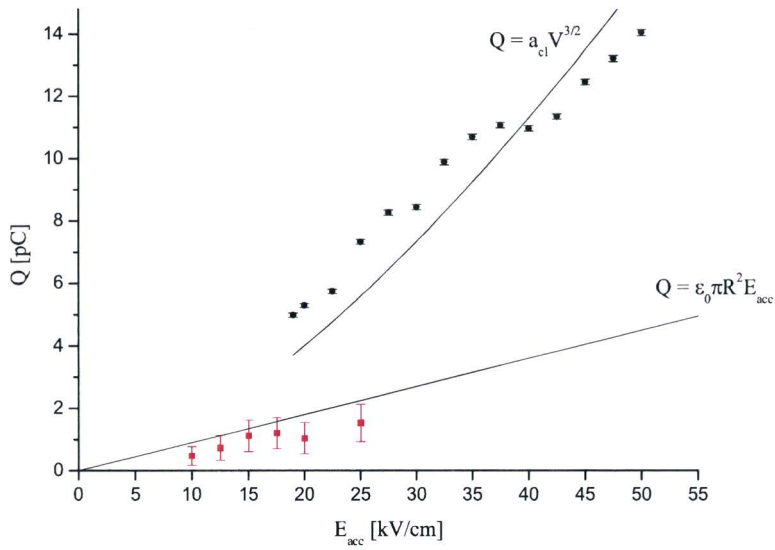
Figure 8.4: *charge as a function of the acceleration field strength. The black dots are measurements without the shaping amplifier, the red squares are measurements with the shaping amplifier. The straight solid line indicates the charge for which the image charge field equals the acceleration field strength. The curved solid line is a fit to the data points of the measurements without the shaping amplifier (black dots).*
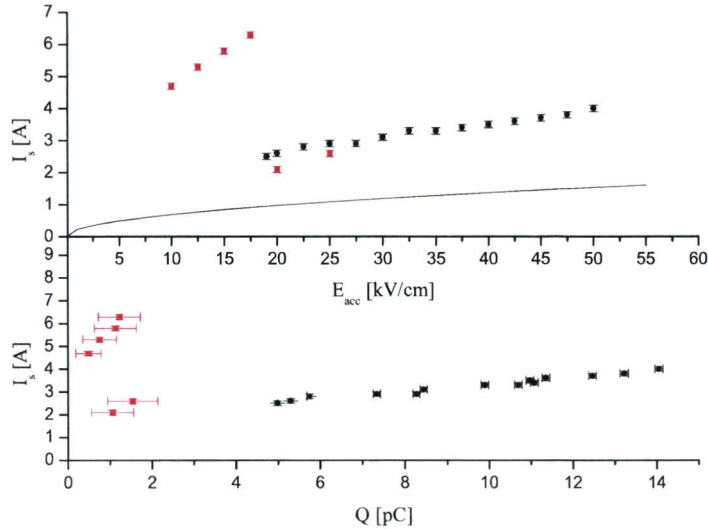
Figure 8.5: *solenoid current as function of charge and as function of acceleration field. The black dots are measurements without the shaping amplifier, the red squares are measurements with the shaping amplifier. The solid line is the solenoid current as a function of the acceleration field as calculated with equations (6.1) and (6.3).*

bunch is known the bunch length can be calculated: $\tau = \frac{0.045 \times 10^{-12}}{0.0364} \frac{1}{A}$. The area A can be determined from the CCD picture as shown in figure 8.3. Because about 80% of the charge is emitted by the brightest spot that area is taken: $A = 2.5 \times 10^{-8} \, \text{m}^2$. The bunch length is then 49 μs, which is indeed longer than the shaping time of 1 μs.

As a check the solenoid current I_s has been measured as a function of the charge and as a function of the acceleration field strength. It should be an increasing function of the acceleration field strength, which is indeed the case. The results are shown in figure 8.5. Also the theoretical graph of I_s as a function of E_{acc} is shown as calculated with equations (6.1) and (6.3). For all measurements without the shaping amplifier, the black dots, the solenoid current is systematically 2.6 ± 0.1 times higher than predicted by theory (see section 6.4). The four measurements with the shaping amplifier, indicated by the red squares, at lowest acceleration fields are inconsistent with the other measurements. These four measurements are systematically 6.9 ± 0.1 times higher than the theoretical value. For both series of measurements a reason for the deviation from theory can be misalignment. If the electron bunch is generated off-axis, then it should be focused into the gap between the two UV incoupling mirrors, see figure 8.1, to capture all electrons in the Faraday cup. When the distance from the center of the bunch to the axis is larger than the radius of iris, the focus has to be in front of the iris as depicted in figure 8.6. The fraction of the bunch that will pass through the iris is then a decreasing function of the focal length. Remember however that the UV spot exists of two separate spots. If the focal length is too short, then the divergence of the second bunch could be so large that it will not pass completely through the iris. So it is likely that there
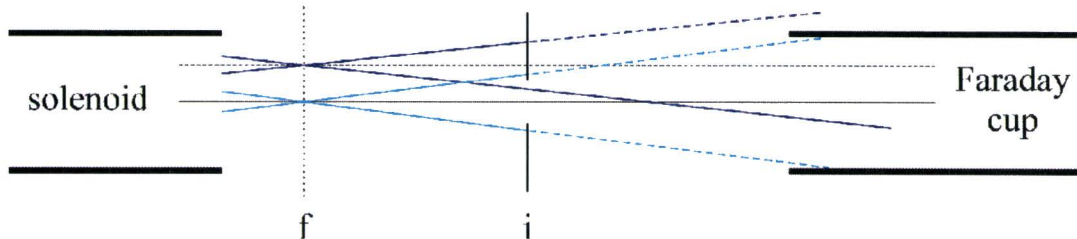
Figure 8.6: *misalignment. One spot (light blue) is on-axis while the other (dark blue) is off-axis. To be collected in the Faraday cup the bunches have to pass through the iris i. For a focal length f of the solenoid part of the off-axis bunch is focused such that it is collected in the Faraday cup. However, a fraction of the on-axis bunch is cut out by the iris and will not be detected.*

exists an optimum focal plane somewhere between the solenoid and the UV mirrors, where the detected charge is maximum.

8.4 Discussion and conclusions

From the two measurements of third order photoemission by back-illumination it is concluded that it would be possible to create bunches of more than $1\,pC$ with the laser system as described in section 5.1. Using ultra-violet laser pulses for front-illumination charges of more than $10\,pC$ can be obtained.

The photocathodes used for back-illumination do not serve. The chromium interlayer (which is needed to enhance adhesion of silver to fused silica) makes that the silver film gets locally damaged during photoemission: at the place of illumination by the laser silver seems to be vaporized. This happens only when the acceleration field is non-zero, so it is not a result of (too) high laser intensities at the cathode. Other experimentalists/research groups have observed the same. The mechanism however is unknown. It is recommended to create new photocathodes without the chromium interlayer and to do the non-linear photoemission experiments by back-illumination again. Another option is to use a copper film instead of silver.

For linear photoemission by front-illumination the constant b_1 is consistent with literature, while the quantum efficiency is one order of magnitude smaller. This can be explained by misalignment so that not all charge has been detected. The UV laser spot actually consists of two spots. It is likely that the contribution to the photoemitted charge of one spot is not or not completely focused into the Faraday cup. The constant b_1 is calculated from the CCD capture of the UV laser spot, not from the charge measurements. Therefore QE can be inconsistent with b_1.

For third order photoemission by back-illumination the non-linear constant is almost two orders of magnitude smaller than that in literature. This can be explained by two reasons. First a result of back-illumination is compared to a result of front-illumination in literature. This counts for a factor 5. Second, differences in calculating the third power of the intensity could be a reason.

Front-illumination with UV laser pulses was done in the space charge limited regime. To create waterbags this is a forbidden regime. Getting out of it can be realized by lowering the laser intensity by enlarging the spot size. When keeping the power of the laser pulses constant the same number of electrons can be photoemitted. Concerning the laser system waterbags with charges up to several tens of pC can then be created. Also when doing back-illumination avoiding the space charge limited regime should be kept in mind.

The solenoid serves well. For 10 pC bunches of an energy of 50 keV the required solenoid current is so low, that air cooling is sufficient to prevent heating problems.

Measuring the signal of the Faraday cup should preferably be done without the shaping amplifier. The accuracy is then up to 5 times higher and ballistic deficit is principally avoided.

Chapter 9

Discussion, conclusions, and outlook

9.1 Discussion and conclusions

When creating high-brightness electron bunches the problem is usually said to be space charge density. However, this is not true. The real problem is the space charge density *distribution*. If the space charge field inside the bunch is a linear function of the position from the center, then the bunch can be compressed transversely and longitudinally to any desired dimension with electro-magnetic lenses, that have sufficiently linear electro-magnetic fields.

A hard-edged 3-D ellipsoid of uniform charge density is the most general distribution for which the space charge field is a linear function of position. Such a bunch is referred to as "waterbag" and is a "Dream Beam" because of its ideal focusability properties. Without loss of generality cylindrically symmetric bunches can be assumed, limiting possible shapes of a waterbag bunch to spheroids. A thin oblate uniformly charged bunch will evolve by its own space charge field into a thicker oblate and finally into a prolate, while remaining uniformly charged. This suggests a way to actually realize a waterbag bunch by starting out with an ultra-thin oblate spheroid, which can be approximated by a pancake bunch. Ultra-short laser pulses are available to create pancake bunches by photoemission. A waterbag bunch can be created by the blow-out of a pancake bunch when three conditions are fulfilled:

1. the final bunch length has to be much larger than the laser pulse length;

2. the acceleration field has to be much larger than the self-field of the bunch;

3. the initial surface charge density distribution σ of the pancake has to be hemisphere-like:
   $\sigma(r) = \sigma_0 \sqrt{1 - (r/A)^2}$.

The final bunch length is determined by the acceleration field strength E_{acc} and by the magnitude of the surface charge density σ_0 of the pancake. The first two conditions together are leading to constraints on the part of the parameter space (σ_0, E_{acc}) for which a pancake bunch will evolve into a waterbag bunch. This is called the *waterbag existence regime*. Particle tracking simulation with the GPT code have been done to find the limits of this existence regime.

To fulfill the third condition, the transverse intensity profile of the laser pulses, which are

used for photoemission, has to be shaped. Simulations with an initial surface charge density distribution as that of a real shaped HeNe laser beam show that practical deviations from the perfect profile are tolerable. Two devices, the piShaper and a SLM-LCD, are proposed to shape the transverse laser profile of ultra-short laser pulses. Longitudinal shaping of the laser pulse is not necessary, because the z-component of the electric field in a pancake bunch is proportional to the *integrated* charge density distribution. This component is therefore independent of the detailed shape of the longitudinal charge density distribution.

An ideal waterbag bunch has linear velocity-position correlations *and* linear field-position correlations. The first is expressed in a low emittance, the latter in a low FL, the field linearity parameter which is defined in section 4.2. Both parameters have to be examined to determine whether a bunch is a waterbag or not.

To demonstrate the waterbag concept a 100 kV DC photogun has been designed and constructed. In practice a maximum voltage of 73 kV is reached, leading to an acceleration field of 8.6 MV/m at the cathode surface. Preliminary photoemission experiments show that with this photogun waterbag bunches with an initial radius of 1 mm and a charge of $1 - -10$ pC can be created, even by non-linear photoemission through back-illumination of thin silver films. Simulations with GPT show that also in the realistic non-uniform acceleration field of the photogun waterbags can be created.

Preliminary results of GPT simulations of longitudinal compression with pillbox RF cavities show that it is possible to compress 1 pC bunches to below 100 fs duration. When these bunches are transversely compressed to 100 μm radius, then ideal bunches for time-resolved electron diffraction are realized. The door would then be opened to study ultra-fast physical, biological, and chemical processes on the timescale of atomic motion by single-shot electron diffraction.

9.2 Outlook

To create waterbag bunches experimentally only one condition still has to be fulfilled: the transverse intensity profile of the laser pulse has to be hemispheric. This can be done in the near future with the piShaper. If necessary also an SLM-LCD has to be bought and used. For efficiency reasons the spatial filter has to be improved so that it would be possible to create bunches of several pC by back-illumination with 800 nm laser pulses. To do this also new photocathodes has to be made without a chromium interlayer between the fused silica substrate and the silver layer. It should also be investigated if a thin copper film is an option. Front-illumination of bulk copper to do either linear or non-linear photoemission is also still an option.

When creating waterbags their experimental realization has to be proven. Therefore diagnostics have to be developed. A phosphor screen can serve to measure the longitudinally integrated transverse profile, which should be hemispherical. The transverse emittance can be measured by sending the bunch through a thin slit and measuring the divergence of the transmitted beam. A streak camera in combination with an energy-spectrometer can be used to measure the energy of the electrons in the bunch as a function of their longitudinal position.

Bibliography

[1] O.J. Luiten et al., *How to realize uniform three-dimensional ellipsoidal electron bunches*, Physical Review Letters, Vol 93 No 9, 2004

[2] P. Smorenburg, *Coherente transitiestraling als basis voor een nieuw type THz-bron*, Technische Universiteit Eindhoven, FTV 2005-05

[3] B.J. Siwick et al., *An atomic-level view of melting using femtosecond electron diffraction*, Science, Vol 302, 21 November 2003

[4] H. Ihee et al., *Direct imaging of transient molecular structures with ultrafast diffraction*, Science, Vol 291, 19 January 2001

[5] F. Schotte et al., *Watching a protein as it functions with 150-ps time-resolved X-ray crystallography*, Science, Vol 300, 20 June 2003

[6] O.J. Luiten, *Beyond the Rf photogun*, published in *The physics and application of high brightness electron beams*, editors J. Rosenzweig et al., World Scientific Publishing, 2003

[7] C. Lejeune and J. Aubert, *Emittance and brightness: definitions and measurements*, published in *Applied charged particle optics*, editor A. Septier, Academic Press, 1980

[8] S. Humphries, *Charged particle beams*, John Wiley & Sons, 1990

[9] E. Durand, *Électrostatique I, Les distributions*, Masson et Compagnie, 1964

[10] L. Serafini, *The short bunch blow-out regime in RF photoinjectors*, AIP Conf. Proc. 413, 1997

[11] C.C. Lin et al., *The gravitational collapse of a uniform spheroid*, Astrophysics Journal, Vol 142 p. 1431 , 1965

[12] http://www.pulsar.nl/gpt

[13] http://www.mt-berlin.com

[14] P.G.E. Lumens, *Laser profile shaping*, Technische Universiteit Eindhoven, FTV 2005-07

[15] J.W. Goodman, *Introduction to fourier optics*, Roberts & Company, 2005

[16] http://www.bnonlinear.com

[17] http://www.hamamatsu.com

[18] J.D. Jackson, *Classical electrodynamics*, John Wiley & Sons, 1999

[19] SUPERFISH is developed and maintained by Los Alamos National Laboratory and can be downloaded for free from LAAGC1.LANL.GOV (IP 204.121.24.18)

[20] L.L. Alston, *High voltage technology*, Oxford University Press, 1968

[21] S. Humphries, *Principles of charged particle acceleration*, John Wiley & Sons, 1997

[22] A. Roth, *Hochspannungstechniek*, Springer-Verlag, 1965

[23] http://www.matsusada.com

[24] H. Zijlstra, *Experimental methods in magnetism, 1. Generation and computation of magnetic fields*, North-Holland Publishing Co., 1967

[25] B.J Siwick, *McGill University, Montreal, Canada*, private communication

[26] W.E. Spicer and A. Herrera-Gómez, *Modern theory and applications of photocathodes*, Techn. Rep. SLAC, SLAC, August 1993 (presented at SPIE's 1993 International Symposium on Optics, Imagaging and Instrumentation, San Diego, 11-16 July 1993)

[27] J.H. Bechtel et al., *Two-photon photoemission from metals induced by picosecond laser pulses*, Physical Review B, Vol 15 No 10, 15 May 1977

[28] R.H Fowler, *The analysis of photoelectric sensitivity curves for clean metals at various temperatures*, Physical Review, Vol 38, 1 July 1931

[29] R. Brogle et al., *Studies of linear and nonlinear photelectric emission for advanced accelerator applications*, IEEE, 1996

[30] D.H. et al., *In-situ cleaning of metal cathodes using a hydrogen ion beam*, 27th Int. FEL Conf. Proc., Stanford, 21-26 August 2005

[31] F.B. Kiewiet, *Generation of ultra-short, high-brightness relativistic electron bunches*, thesis, Technische Universitcit Eindhoven, 2003

[32] A. Damascelli et al. *Multiphoton electron emission from Cu and W: an angle-resolved study*, Physical Review B, Vol 54 No 9, 1 September 1996

[33] J.D. Lawson, *Physics of charged-particle beams*, Ofxord University Press, 1988

[34] *Handbook of accelerator physics and engineering*, editors A. Wu chao and M. Tigner, World Scientific Publishing, 1999